

RESEARCH ARTICLE

10.1002/2014JF003421

Stochastic interpretation of the advection-diffusion equation and its relevance to bed load transport

C. Ancey¹, P. Bohorquez², and J. Heyman¹¹School of Architecture, Civil and Environmental Engineering, École Polytechnique Fédérale de Lausanne, Lausanne, Switzerland, ²Área de Mecánica de Fluidos, Universidad de Jaén, Campus de las Lagunillas, Jaén, Spain

Key Points:

- Stochastic derivation of the advection diffusion equation
- Nonlocal effect induced by stochastic advection
- Approximation of this effect by an artificial diffusivity

Supporting Information:

- Text S1
- Figure S2
- Figure S3
- Figure S4
- Figure S5
- Figure S6
- Figure S7
- Figure S8
- Figure S9
- Figure S10
- Figure S11
- Figure S12
- Figure S13
- Figure S14
- Figure S15
- Figure S16
- Figure S17
- Figure S18
- Figure S19
- Figure S20

Correspondence to:

C. Ancey,
christophe.ancey@epfl.ch

Citation:

Ancey, C., P. Bohorquez, and J. Heyman (2015), Stochastic interpretation of the advection-diffusion equation and its relevance to bed load transport, *J. Geophys. Res. Earth Surf.*, 120, doi:10.1002/2014JF003421.

Received 22 DEC 2014

Accepted 2 NOV 2015

Accepted article online 6 NOV 2015

Abstract The advection-diffusion equation is one of the most widespread equations in physics. It arises quite often in the context of sediment transport, e.g., for describing time and space variations in the particle activity (the solid volume of particles in motion per unit streambed area). Phenomenological laws are usually sufficient to derive this equation and interpret its terms. Stochastic models can also be used to derive it, with the significant advantage that they provide information on the statistical properties of particle activity. These models are quite useful when sediment transport exhibits large fluctuations (typically at low transport rates), making the measurement of mean values difficult. Among these stochastic models, the most common approach consists of random walk models. For instance, they have been used to model the random displacement of tracers in rivers. Here we explore an alternative approach, which involves monitoring the evolution of the number of particles moving within an array of cells of finite length. Birth-death Markov processes are well suited to this objective. While the topic has been explored in detail for diffusion-reaction systems, the treatment of advection has received no attention. We therefore look into the possibility of deriving the advection-diffusion equation (with a source term) within the framework of birth-death Markov processes. We show that in the continuum limit (when the cell size becomes vanishingly small), we can derive an advection-diffusion equation for particle activity. Yet while this derivation is formally valid in the continuum limit, it runs into difficulty in practical applications involving cells or meshes of finite length. Indeed, within our stochastic framework, particle advection produces nonlocal effects, which are more or less significant depending on the cell size and particle velocity. Albeit nonlocal, these effects look like (local) diffusion and add to the intrinsic particle diffusion (dispersal due to velocity fluctuations), with the important consequence that local measurements depend on both the intrinsic properties of particle displacement and the dimensions of the measurement system.

1. Introduction

This article is concerned with the microscopic foundation of the advection-diffusion equation with a source term

$$\frac{\partial c}{\partial t} + \bar{u}_p \frac{\partial c}{\partial x} = s(c) + D \frac{\partial^2 c}{\partial x^2} \quad (1)$$

As we will mainly study this equation in the context of sediment transport, $c(x, t)$ denotes the solid volume of particles in motion per unit streambed area (m). Following *Furbish et al.* [2012a], we refer to c as *particle activity*. We will focus on one-dimensional problems and so c is expressed as a function of the position x along the streambed and time t . The second term on the left-hand side represents advection and \bar{u}_p is the *advection velocity* (m s⁻¹), i.e., the mean velocity of particles when sediment is in motion. The first contribution to the right-hand side represents the source term, here the net balance between the entrainment and deposition rates of particles from/on a streambed. In this paper, we will focus on linear processes, and so we assume that the source term s (m s⁻¹) is either independent of c or a linear function of c (see section 2.2). The second term on the right-hand side of equation (1) is the diffusion process, with D the *particle diffusivity* (m s⁻²). The physical interpretation of the advection-diffusion equation (1) is straightforward: particle activity varies with time as a result of transport by the water stream (advection), spreading (dispersion or diffusion due to particle velocity fluctuations), and mass transfer with the streambed (entrainment and deposition).

The advection-diffusion equation is one of the most widespread equations in physics and related sciences. In Earth surface processes related to sediment transport, it arises in different forms and in various contexts

such as soil creep and erosion [Culling, 1960; Furbish and Haff, 2010], landscape evolution [Paola, 2000; Martin, 2000; Tucker and Bradley, 2010; Salles and Duclaux, 2015], bed load transport [Parker et al., 2000; Lajeunesse et al., 2010; Furbish et al., 2012b; Ancey and Heyman, 2014; Pelosi et al., 2014], suspended transport [van Rijn, 2007], solute transport [Bencala and Walters, 1983; Boano et al., 2007], and wave-induced sediment transport [Blondeaux et al., 2012]. Diffusion is also at the core of many investigations on suspension and bed load transport [Oh and Tsai, 2010; Seizilles et al., 2014], hillslope sediment transport [Heimsath et al., 2005; Foufoula-Georgiou et al., 2010], evolution of braiding rivers [Reitz et al., 2014], and tracer behavior [Nikora et al., 2002; Ganti et al., 2010; Martin et al., 2012; Roseberry et al., 2012; Lajeunesse et al., 2013].

The advection-diffusion equation (1) is a macroscopic equation that is often postulated without reference to any microscopic analysis. It can certainly be derived from conservation principles of continuum mechanics (conservation of mass) and phenomenological laws (Fickian dispersion law, reaction rate equation) [Crank, 1975], but its basis remains essentially empirical. While a postulation approach has the advantage of simplification, it fails to provide strong justification for the relevance of equation (1) to a particular setting and there is no general method for determining the various parameters involved in equation (1), their possible interconnection, and their parametric dependence on sediment properties. A microscopic underpinning of macroscopic models such as equation (1) has several advantages. First, the various terms appearing in macroscopic equations can be shown to arise from microscopic processes. For instance, in the Reynolds-averaged Navier-Stokes equations, the Reynolds stress tensor (representing fluid turbulence) arises from the fluctuating velocity field, and awareness of this connection is key to understanding and modeling turbulence [Pope, 2000]. By averaging microscopic equations to derive their macroscopic counterparts, we can find out contributions that would have been omitted in the postulated model and give insights into the terms expected to play a significant part on the macroscopic scale. Second, to simplify the problem by reducing the amount of information, some sort of averaging process has to be applied to derive macroscopic equations from microscopic considerations, which makes it possible to relate the resulting macroscopic variables to local properties [Batchelor, 1974]. For instance, when studying the dispersion of matter in turbulent fluid or the flow of neutrally buoyant particle suspensions, the particle diffusivity can be linked with the flow features [Majda and Kramer, 1999; Guazzelli and Morris, 2012; Gillespie and Seitaridou, 2013]. Third, the averaging process often raises important questions about the representative length and time scales of the problem at hand: the nature of transport phenomena resolved by macroscopic equations depends a great deal on the scale at which the process is observed. For instance, a particle undergoing Brownian motion sees its velocity and displacement direction change many times per unit time (and so the resulting path is well captured by a stochastic Langevin equation), but if we observe it on a shorter timescale, the random walk with uncorrelated steps reveals a continuous ballistic path (in that case, a deterministic model is more suited to describing particle motion) [Pusey, 2011].

The aim of this paper is to propose a microscopic framework for the advection-diffusion equation (1). To this end, we revisit our theoretical framework with an emphasis given to advection: in our earlier publications, we have shown that the theory of birth-death Markov processes is well suited to describing the statistical properties of sediment transport [Ancey et al., 2006, 2008]. The model was then extended to derive a continuum version [Ancey, 2010] and include diffusive effects induced by particle velocity fluctuations [Ancey and Heyman, 2014]. The model has been recently coupled with the Saint-Venant equations to study bed form initiation and antidune migration under supercritical flow conditions [Bohorquez and Ancey, 2015]. Comparison with experimental data has also been presented in earlier publications [Ancey et al., 2008; Heyman et al., 2013, 2014].

Two elements are of particular significance to the present microscopic analysis. First, we emphasize the part played by fluctuations (of sediment transport rate, particle activity, and bed elevation) in the dynamics of sediment transport. Section 1.1 shows how large the fluctuations of sediment flux can be relative to the mean flux and how this affects measurement and modeling. The key question is to what extent sediment transport—seen as a macroscopic transport process—is affected by noise (i.e., the fluctuations on the microscale). On the whole, there are two possible answers: (i) noise is irrelevant on large scales so that the fluctuation effects on the macroscopic behavior can be either ignored or modeled using a closed-form representation, e.g., the term for particle diffusion in equation (1) and (ii) noise is relevant on large scales, with the consequence that the fluctuation effects are expected to appear in the macroscopic governing equation in a nonclosed form and thus they are part of the problem to be solved (the Reynolds stress tensor in the Reynolds-averaged Navier Stokes equation is a case in point). We will see that depending on flow

conditions, sediment transport falls under (i) or (ii). The good news is that even in case (ii), an approximate closure equation for the fluctuation effects can be proposed. Second, the problem under investigation changes nature between the microscale and macroscale: at the particle scale, sediment transport is a discrete problem, while on the bulk scale, it is considered a continuum problem. For particulate systems characterized by a clear separation of length scales, this change does not cause trouble as any elementary volume contains a sufficiently large number of particles for the continuum approximation to hold. In contrast, for bed load transport problems, for which this separation of scales may be hardly applicable, the usual definitions of particle flux and concentration used in continuum mechanics run into practical difficulties, as noted by *Furbish et al.* [2012b], *Ballio et al.* [2014], and others. Following the standard procedure in continuum mechanics, we will describe the microscopic behavior by considering control volumes, then take the ensemble average and continuum limit to derive the advection-diffusion equation (1). In doing so, we will demonstrate that applying the continuum equation (1) to practical problems is potentially fraught with error because of the combined effects of fluctuations and length scales: difficulties arise in the treatment of the advection term between the microscale and macroscale, which may cause the diffusion coefficient D to be scale dependent when the integral form (over control volumes) or discretization of equation (1) is used.

There have been a few attempts to build a microscopic framework for the advection-diffusion equation (1) in the context of particle transport. We review these efforts in section 1.2. The main originality of the paper is that we focus on the Eulerian approach, in which we choose a specific location x in space and monitor the changes in the particle activity c with time t within a control window centered at x . The paper is organized as follows. Section 2 summarizes the theoretical framework for modeling sediment transport on microscales and deriving the advection-diffusion equation (1) for particle activity. In section 3, we present numerical simulations showing the difference between the discrete and continuum formulations in the particular case of pure advection (particles move at constant velocity). In section 4, we show how the results are modified when particle agitation (reflecting fluctuating particle velocities) is taken into account. This paper contains a rich amount of mathematical material. In order to present the main concepts and results within limited space, we have skipped the mathematical detail. However, all mathematical proofs are presented in the supporting information, and the interested reader can follow the cross references to find further information. In the present paper, emphasis is given to theoretical tools and we refer the reader to our companion papers to see practical applications [*Bohorquez and Ancey*, 2015; *Heyman et al.*, 2014; *J. Heyman et al.*, Exploring the physics of sediment transport in nonuniform supercritical flows through a large data set of particle trajectories, submitted to *Journal of Geophysical Research*, 2015]. An explanatory list of the notation used in this paper accompanies the appendices.

1.1. Sediment Transport and Fluctuations

Sediment transport exhibits considerable spatial and temporal fluctuations. A typical example of this variability is given by Figure 1, which shows the time variation in the sediment transport rate for a gravel bed flume experiment under steady state conditions (see Appendix A for further information on the experimental conditions). The resulting time series illustrates various features of sediment transport at low transport rates: while the experiment was run for a very long time (more than 50 h), the system did not reach a steady state characterized by gentle fluctuations around a fixed value but seemed to jump from states marked by low sediment transport activity (possibly with transport rates dropping to zero) to phases of intense sediment transport (with transport rates as large as 20 times the feeding rate). The bursts are likely to reflect the migration of bed forms (here antidunes) [*Gomez*, 1991].

For systems of this kind, fluctuations are likely to play an important part in the overall dynamics. Understanding the part played by fluctuations in sediment transport is key to various issues such as measurement of bed load transport rates and development of realistic morphodynamic models. We will outline these two problems below.

For a very long time, the effect of fluctuations on the measurement of transport rates has gone unnoticed. In recent decades, with the development of high-resolution techniques for measuring transport rates both in the laboratory and in the field, it has been shown that the results depend a great deal on sampling time [*Cudden and Hoey*, 2003; *Bunte and Abt*, 2005; *Singh et al.*, 2009; *Campagnol et al.*, 2012; *Gaeuman et al.*, 2015].

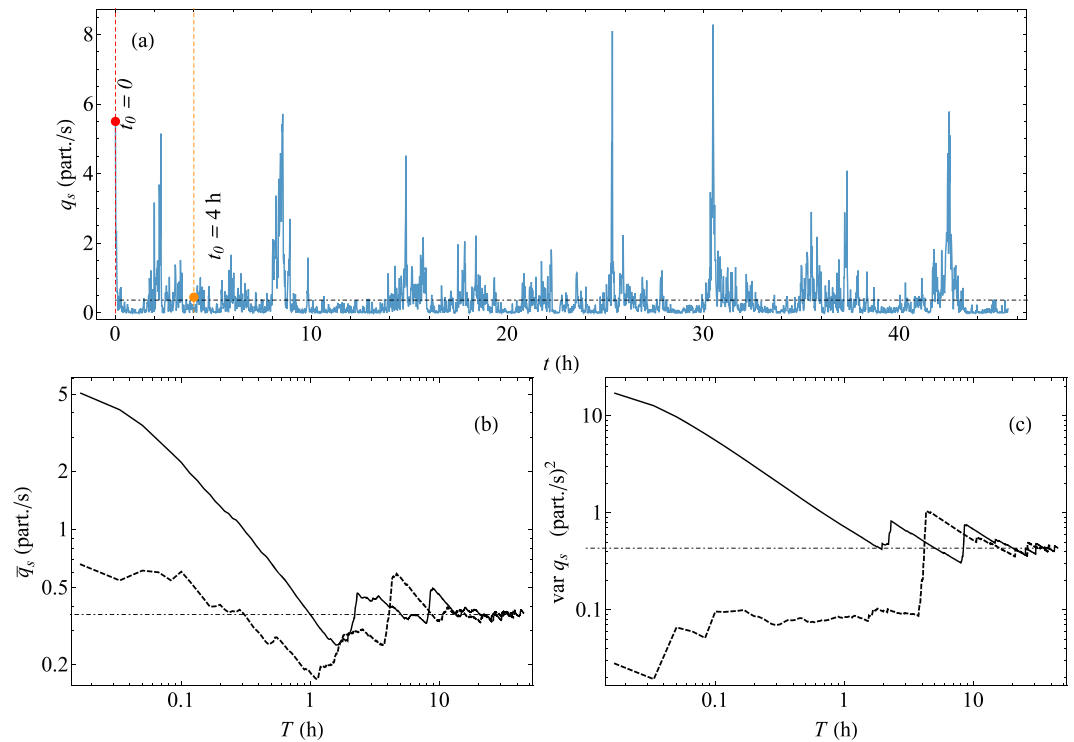


Figure 1. (a) Particle transport rate q_s as a function of time. (b) Variation of the time-averaged particle transport rate as a function of the integration time; the solid line shows the empirical curve $\bar{q}_s(T; t_0)$ when the starting time is $t_0 = 0$, while the dashed line represents the $\bar{q}_s(T; t_0)$ for $t_0 = 4$ h. The dash-dotted line shows the sample mean $m = 0.366$ pps. (c) Variation of the variance of the particle transport rate $\text{var } q_s(T; t_0) = \frac{1}{T} \int_{t_0}^{t_0+T} (q_s(t) - m)^2 dt$ as a function of the integration time. See Appendix A for the experimental conditions and experimental procedure. Time series data available from <http://dx.doi.org/10.6084/m9.figshare.1480646>.

Closely related is the question of the optimum sampling time for a given setting, a problem that has as yet few solutions. Figure 1b shows the time-averaged transport rate for the time series $q_s(t)$ shown in Figure 1a

$$\bar{q}_s(T; t_0) = \frac{1}{T} \int_{t_0}^{t_0+T} q_s(t) dt \tag{2}$$

with T the sampling time and t_0 the starting time. For this experiment, the time-averaged transport rate converged very slowly to the mean sample m : T must be as long as 2 h for \bar{q}_s to come close to m to within $\pm 20\%$. Even for very long times ($2 < T < 15$ h), \bar{q}_s can deviate markedly from the mean sample as a result of bed form migration (the two peaks of \bar{q}_s at $T = 2$ h and 9 h were associated with bed form development). Similar conclusions can be drawn for the time-averaged variance, which slowly converges to the sample variance (see Figure 1c). Figure 1 also shows that the empirical curve $\bar{q}_s(T)$ depends a great deal on the starting time. If we start integrating q_s when sediment transport is intense (e.g., $t_0 = 0$ in Figure 1), the time-averaged sediment transport rate deviates initially by a factor 10 from the sample mean m . It comes as no surprise that if we select the starting time (e.g., $t_0 = 4$ h in Figure 1) so that sediment transport is initially low, then the time-averaged sediment transport rate \bar{q}_s deviates less markedly from m . This example also demonstrates that the question of the optimal sampling time for evaluating sediment transport rate has no clear-cut answer.

This particular example shows that in contrast with many fluctuating processes, the mean transport rate cannot be estimated by merely smoothing the measurements over a short time span. It can require long sampling times even under steady state conditions (especially at low sediment transport rates) and so the question arises as to how to determine proper estimates of \bar{q}_s under time-dependent flow conditions, e.g., when the timescale of water discharge changes is shorter than the optimum sampling time of \bar{q}_s .

The effect of sampling time on transport rate measurement is becoming even more apparent with field data. *Recking et al.* [2012] tested different bed load transport equations against instantaneous field measurements, volume accumulated at the event scale, volume accumulated at the annual and interannual scales,

and time-integrated flume measurements. At the shortest timescales (say, a few minutes), all of the bed load equations tested failed to predict the mean sediment transport rate to within one order of magnitude. The results were especially poor for coarse-bed rivers and steep slopes. In contrast, on much longer timescales (say, 1 year), the predictions more closely matched the field data, with relative errors (defined as the computed to measured sediment volume ratio) lower than five in most cases.

Existing morphodynamic models are based on equations such as the advection-diffusion equation (1). More elaborate models are composed of a set of governing equations. For instance, the Saint-Venant-Exner equations consist of mass and momentum balance equations for streamflow, sediment transport, and bed elevation, supplemented by closure equations for estimating flow resistance [García, 2007]. In all of these models, the flow variables are smooth (or piecewise continuous) fields. In other words, these models do not provide instantaneous values, but spatially or temporally averaged values. The effects of random perturbations on the mean flow are either ignored or incorporated in the form of a diffusive term (the equivalent of the eddy diffusion process in turbulence models). Owing to the random nature of sediment transport rates, morphodynamic models are fraught with difficulties of different order.

The first impediment has been highlighted by Figure 1. Any direct comparison between theory and observation is made quite difficult because of the great sensitivity of the mean sediment transport rate to sampling time. In practice, this hurdle has mostly been avoided by looking at global patterns such as the determination of the areas prone to aggradation/degradation or the evaluation of the sediment budget over a long characteristic time [e.g., see Ferguson and Church, 2009].

Another difficulty arises when solving morphodynamic models numerically. Finite-volume methods are preferentially used for several reasons. First of all, discretization based on finite volumes is seen as more physical as the resulting discretized equations are obtained by integrating the governing equations over elementary control volumes, expressing the flux (e.g., mass and momentum) through the boundaries of each volume, and updating the volume-averaged quantities [LeVeque, 2002; Toro, 2001]. A clear advantage of this computational strategy is the possibility to deal with discontinuities (e.g., a hydraulic jump). As the method makes use of volume averaging, it suffers from mesh size dependence when applied to random fields in the same way as the time-averaged sediment transport rate (2) depends on sampling time. This subtle point will be illustrated in the following; the reader is also referred to our companion paper for further discussion on this point [Bohorquez and Ancey, 2015].

1.2. Existing Approaches to Deriving the Advection-Diffusion Equation

Equation (1) is often derived using conservation principles of continuum mechanics and phenomenological laws. Arguments of this sort have been used to derive an advection equation for particle activity [Charru, 2006; Lajeunesse et al., 2010]. The main shortcoming of this approach is that it ignores or downplays the fluctuations of particle activity and its crucial influence on the sediment transport dynamics.

There is a considerable literature on the microscopic foundation of the advection-diffusion equation and much of this literature makes use of the Lagrangian approach to derive equation (1) [Méndez et al., 2010; Gillespie and Seitaridou, 2013] with consideration for fluctuations of particle motion. Essentially, in this approach, a target particle is tracked. On the microscale, the erratic and intermittent motion of this particle can be described using random walk models. Lagrangian models include a wide variety of processes depending on the working assumptions: the particle motion can be seen as a series of jumps of fixed or random length occurring at fixed or random times [Metzler and Klafter, 2000; Schumer et al., 2009]. The Lagrangian approach has applications of particular relevance to suspending particles in rivers [Oh and Tsai, 2010; Tsai et al., 2014], bed load transport [Einstein, 1950; Furbish et al., 2012a, 2012b, 2012c; Pelosi et al., 2014], tracers [Ganti et al., 2010; Hill et al., 2010; Zhang et al., 2012], and hillslope sediment transport [Furbish and Roering, 2013]. The simplest model is the discrete-time random walk where the target particle moves intermittently and may jump to the left or the right (see section 1 in the supporting information). The hops are of fixed length and occur at discrete times. This very simple configuration is sufficient to derive equation (1) in the absence of source ($s = 0$) and link the advection velocity and diffusivity to the jump features. More elaborate models lead to the advection-diffusion equation with a source term (1) [Méndez et al., 2010]. Note that in the field of sediment transport and river morphology, the Lagrangian approach leads to macroscopic equations that are more

complicated than the classic advection-diffusion equation (1). For instance, *Furbish et al.* [2012b] show that ensemble-averaged particle transport rate takes the form

$$\langle q_s \rangle(x, t) = c\bar{u}_p - \frac{1}{2} \frac{\partial}{\partial x}(Dc) \quad (3)$$

Mass conservation for the bed implies that

$$\frac{\partial}{\partial x} \langle q_s \rangle = \mathcal{E}(x, t) - D(x, t) = \frac{\partial}{\partial x}(c\bar{u}_p) - \frac{1}{2} \frac{\partial^2}{\partial x^2}(Dc) \quad (4)$$

where \mathcal{E} and D are the entrainment and deposition rates, respectively. Equation (4) contains advection and diffusion terms like equation (1), but there is no temporal variation $\partial_t c$ and the source term $s = \mathcal{E} - D$ is a priori not a simple linear function of c .

With regards to the Eulerian microscopic foundation of the advection-diffusion equation (1), there is a considerable body of work related to diffusion-reaction equations, i.e., equation (1) with a vanishing advection velocity $\bar{u}_p = 0$ [Gardiner, 1983; Isaacson, 2005; Hellander et al., 2012]. Yet, surprisingly, we failed to find articles including advection in the diffusion-reaction equation and, even more surprisingly, our preliminary investigations showed us that the inclusion of advection in equation (1) leads to unexpected difficulties of interpretation. The explanations are numerous. First, the mathematics underpinning the stochastic derivation of equation (1) are still an emerging field. The fundamentals of stochastic differential equations are now well established [Higham, 2001; Allen, 2007], and they have been of common use for many years in physics, mathematical finance, and biology [Gardiner, 1983; Gillespie, 1992; Platen, 1999; Iacus, 2008]. In contrast, there is a greater potential for difficulties with stochastic partial differential equations. Reaction-diffusion equations in chemical physics are a typical example of how different working assumptions on the structure of the noise term lead to quite different governing equations [Gardiner, 1983; Dogan and Allen, 2011]. Numerical solutions to the stochastic Burgers equation (a nonlinear variant of the advection-diffusion equation) highlight the influence of the mesh size on the solution to which the numerical schemes converge, a situation that contrasts with the deterministic case [Hairer and Voss, 2011]. The interpretation of white noise (Itô versus Stratonovich convention) relies on a working assumption that may also lead to conceptual and mathematical difficulties depending on the rule chosen [Ridolfi et al., 2011] (see also section 2.3).

2. Markovian Eulerian Framework

Before tackling the question of the stochastic foundation of the advection-diffusion (1) (see section 2.3), we summarize our approach presented in earlier papers [Ancey et al., 2008; Ancey and Heyman, 2014]. A convenient framework for the investigation of the statistical properties of sediment transport is the theory of birth-death Markov processes, which has been quite successful in various fields such as population dynamics, epidemiology, and chemical kinetics [Cox and Miller, 1965; Gillespie, 1992]. We think that it can also be a very powerful tool to better understand the dynamics of sediment transport.

2.1. Outline of the Approach

We are interested in studying the variation in the particle activity $c(x, t)$ along a river. For the sake of simplicity, we consider a one-dimensional stream and ignore any cross-stream variation. On the microscopic scale, the particle activity is linked to the number of moving particles N contained in a (control) volume of length Δx . The idea underpinning the Markovian Eulerian framework is a general and rather intuitive one, which consists in monitoring the changes in the number moving particles over a time interval Δt within this control volume. This number N can vary because particles can be entrained from the bed, deposited on the bed, enter the volume, or leave it. These events occur randomly and a priori independently and so N is a discrete random variable described by a probability $P(n, t)$ of observing $N = n$ particles within the volume at time t . We study a subclass of Markov processes called *birth-death* processes, for which the number of particles can only experience jumps of $+1$ or -1 , which means in practice that the time interval Δt must be short enough to allow the detection of such jumps. Sediment transport is assumed to be sufficiently low for events to be distinguishable. At higher sediment transport rates, multiple events (erosion, deposition, emigration, and immigration) can occur within infinitesimal times, making the present stochastic framework irrelevant. In the present context, *emigration* and *immigration* refer to moving particles that leave or enter the control volume.

Our approach is *Eulerian* in that we do not track particles individually, but merely count the number of particles in a control volume. It is *Markovian* because we assume that the variations in N in the time interval t and $t + \Delta t$

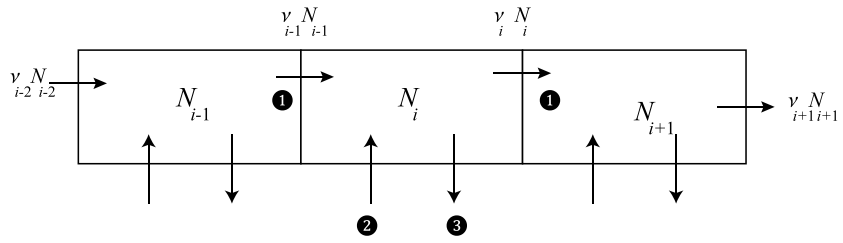


Figure 2. Entrainment, deposition, and transport of particles in an array of cells of length Δx .

depend primarily on Δt . Said differently, we do not need the complete history of N up to time t to determine what may happen in the time interval t and $t + \Delta t$. It is *discrete* because we consider a collection of finite-size particles within a control volume of finite length Δx .

In this section, our goal is to determine the governing equation of $N(t)$ as a function of the volume length Δx and time step Δt , then to derive a differential (macroscopic) equation for particle activity in the continuum limit (i.e., as the parameters Δx and Δt approach zero).

2.2. Mass Balance and Governing Equation at the Particle Scale

We split the one-dimensional stream into an array of M cells i of length Δx and we monitor the number of moving particles N_i in each cell (see Figure 2). More specifically, we are interested in calculating $P(\mathbf{n}; t) = \text{Prob}(\mathbf{N} = \mathbf{n}; t)$ the probability of observing $\mathbf{n} = (n_1, \dots, n_M)$ particles in each cell at time t . The vector \mathbf{N} represents the state of the system. Like in continuum mechanics (in its integral formulation), we will perform the mass balance for each cell by counting the particles entrained, deposited, or leaving the cells over a short time span δt .

Yet there are two crucial elements that distinguish the stochastic approach from the continuum approach: when tracking particles, we evaluate their probabilities of changing state or position and that is why we calculate $P(\mathbf{n}; t)$ and not $\mathbf{N}(t)$. The second point is that the time increment is not arbitrary: it must be sufficiently small so that there cannot be two or more processes occurring across the whole array between times t and $t + \delta t$.

To complete our introduction, we need some extra symbols to characterize the change of state $\Delta \mathbf{N}$ within $[t, t + \delta t)$: \mathbf{r}_i^j is a vector in which all but two entries are zero: $r_i = 1, r_j = -1, r_k = 0$ for $k \neq i, j$. This symbol denotes a displacement of a particle from cell j to cell i . \mathbf{r}_i^\pm is a vector in which all but one entries are zero: $r_i = \pm 1, r_k = 0$ for $k \neq i$. It reflects entrainment or deposition within cell i .

We use the following assumptions to derive the governing equation for $P(\mathbf{n}; t)$. First, we assume that once set into motion, the particles move at the same velocity \bar{u}_p . This assumption will be relaxed in the following (see section 4), but as a first step, it allows us to make the picture simpler by distinguishing between the effects due to particle advection (mean displacement) and particle fluctuation (velocity fluctuations) at the bulk scale. Note that the assumption of constant velocity does not imply that the motion of the particles is purely deterministic because at any time, part of the moving particles will be deposited on the bed while other particles will be dislodged from the bed and join the cloud. All particles have the same size and so there is no grain sorting. We do not distinguish between rolling and saltating motions even though there is experimental evidence that the type of motion plays a role in sediment transport dynamics [Ancey *et al.*, 2006; J. Heyman *et al.*, submitted manuscript, 2015] since rolling and saltating particles do not move at the same velocity.

A consequence of advection is that at any time, part of the moving particles contained in cell i will leave this cell and enter cell $i + 1$. Note that at this stage of the development, we assume that the time step δt is so small that the displacement $\bar{u}_p \delta t$ cannot exceed the cell length and so particles can jump from one cell to its downstream neighbor, but cannot make long hops. We thus impose the constraint $\bar{u}_p \delta t < \Delta x$, which can be interpreted as a Courant-Friedrichs-Lewy (CFL) condition for the jump process. The probability that one particle leaves cell $i - 1$ and enter cell i is denoted by

$$p_i^1 = \text{Prob}(\mathbf{N} = \mathbf{n} + \mathbf{r}_i^{i-1}; t + \delta t) = v_{i-1} N_{i-1} \delta t \tag{5}$$

where $v_{i-1} = \bar{u}_p / \Delta x$ (s^{-1}) is the emigration rate for cell $i - 1$. The superscript 1 in p_i^1 indicates that it is the first process we include in our study. If the particles are uniformly distributed inside cell $i - 1$, the probability that

an individual particle leaves the cell over the time step δt is $\bar{u}_p \delta t / \Delta x$. Since they are N_{i-1} particles in cell $i-1$, the resulting probability is then given by equation (5).

Particles can be entrained and deposited. We assume that the entrainment and deposition rates, \mathcal{E} (particles per second (pps)) and \mathcal{D} (pps), respectively, can be expanded as a power series of N

$$\mathcal{E} = \mathcal{E}_0 + \mathcal{E}_1 N + \dots \quad (6)$$

$$\mathcal{D} = \mathcal{D}_0 + \mathcal{D}_1 N + \dots \quad (7)$$

As we investigate linear models, the expansions are limited to order 1. Concerning deposition, as there are N moving particles, the deposition rate is necessarily linearly dependent on N and so $\mathcal{D}_0 = 0$. To keep the notation consistent with our earlier papers [Ancey *et al.*, 2008; Ancey and Heyman, 2014], we denote \mathcal{D}_1 by σ (s^{-1}); we index it by i to recall that σ depends on position. The probability of deposition in cell i is then

$$p_i^2 = \text{Prob}(\mathbf{N} = \mathbf{n} + \mathbf{r}_i^-; t + \delta t) = \sigma_i N_i \delta t \quad (8)$$

For entrainment, we interpret \mathcal{E}_0 as the effect of the water stream alone on the bed. Moving particles induce perturbations, collisions, changes in the water turbulence, etc., which can also lead to dislodge particles from the bed. We refer to the coefficient \mathcal{E}_1 as *collective entrainment*, but this name is confusing to some degree as it may lead one to think that several particles are simultaneously entrained. This is not the meaning here (massive entrainment would conflict with our working assumption that there is no more than one event over the time span δt). Again, for consistency with our earlier publications [Ancey *et al.*, 2008; Ancey and Heyman, 2014], we denote \mathcal{E}_0 and \mathcal{E}_1 by λ (pps) and μ (s^{-1}). The probability of entrainment in cell i is thus

$$p_i^3 = \text{Prob}(\mathbf{N} = \mathbf{n} + \mathbf{r}_i^+; t + \delta t) = (\lambda_i + \mu_i N_i) \delta t \quad (9)$$

In equations 5, (8), and (9), we have calculated the transition probabilities p_i^k ($k = 1, 2$, and 3) that process k occurs in cell i ($1 \leq i \leq M$). We can now calculate the probability of change for the whole system. We will not reproduce the derivation of the governing equation, which can be found in our earlier papers [Ancey *et al.*, 2008; Ancey and Heyman, 2014]. The fundamental idea is that starting from the Chapman-Kolmogorov equation

$$P(\mathbf{n}, t + \delta t) = \sum_{\text{for all } \Delta \mathbf{n} \text{ and } k=1,2,3} P(\mathbf{n} + \Delta \mathbf{n}, t) p^k(\mathbf{n} + \Delta \mathbf{n} \rightarrow \mathbf{n}, \delta t) \quad (10)$$

and taking the limit $\delta t \rightarrow 0$, we end up with the *forward Kolmogorov equation* (also called the master equation)

$$\begin{aligned} \frac{\partial P}{\partial t}(\mathbf{n}; t) = & \sum_{i=1}^M (n_i + 1) (P(\mathbf{n} + \mathbf{r}_{i+1}^j, t) v_i + P(\mathbf{n} + \mathbf{r}_i^+, t) \sigma_i) \\ & + P(\mathbf{n} + \mathbf{r}_i^-, t) (\lambda_i + \mu_i (n_i - 1)) \\ & + P(\mathbf{n} + \mathbf{r}_i^{j-1}, t) v_{i-1} n_{i-1} \\ & - P(\mathbf{n}, t) (v_{i-1} n_{i-1} + \lambda_i + \mu_i n_{i+1} + v_i n_i + \sigma_i n_i) \end{aligned} \quad (11)$$

which is the governing equation for \mathbf{N} .

Apart from the one-cell case ($M = 1$) [Ancey *et al.*, 2008], there is no technique for solving this equation analytically. In this respect, the governing equation (11) for \mathbf{N} does not allow us to directly derive a macroscopic equation for N in the form of an advection-diffusion equation. However, various techniques can be used for finding numerical solutions and analytical approximations and for transforming the forward Kolmogorov equation (11) into a more tractable form (see sections 2 and 3 in the supporting information). In the following, we will use an exact technique (the Poisson representation) to transform the forward Kolmogorov equation (11) to gain analytical traction. Direct numerical solutions of the forward Kolmogorov equation (11) are also possible [Gillespie, 1992, 2001; Lipshtat, 2007; Pineda-Krch, 2008].

2.3. Derivation of the Ensemble-Averaged Equation for Particle Activity c

To proceed with the determination of solutions to equation (11), we use an elegant and exact technique, which can be thought of as a Laplace-like transform: the *Poisson representation* makes it possible to pass from

Table 1. Correspondence Between the Variables Used

	Real World	Poisson transform	Poisson Space
Discrete random variable	N		a
	number of moving particles		Poisson rate
Continuous random variable	$\gamma = \lim_{\Delta x \rightarrow 0} \frac{N}{\Delta x}$		$b = \lim_{\Delta x \rightarrow 0} \frac{a}{\Delta x}$
	particle activity		Poisson density
Ensemble-averaged variable	$c = \langle \gamma \rangle$		
	mean particle activity		

the discrete random variable \mathbf{N} to the (dimensionless) continuous random variable \mathbf{a} (here called the *Poisson rate*) [Gardiner, 1983]

$$P(\mathbf{n}, t) = \prod_i \int_{\mathbb{R}_+} \frac{e^{-a_i} a_i^{n_i}}{n_i!} f(\mathbf{a}, t) d\mathbf{a} \quad (12)$$

where $\mathbf{a} = (a_i) \geq 0$ for $i = 1, 2, \dots$ and $f(\mathbf{a}, t)$ is the multivariate probability density function of \mathbf{a} . Instead of working with the discrete random variable \mathbf{N} , we now work with the continuous random variable $\mathbf{a} = (a_1, a_2, \dots)$. It is often more convenient to work in another functional space to simplify the equations (like Fourier and Laplace transforms), but the way back to the original space may be impossible. Here we will avoid this issue by using an interesting feature of the Poisson representation, which is the relationship between the p factorial moments of N and the p moments of a . In particular, we have

$$\langle N \rangle = \langle a \rangle \text{ and } \text{var } N = \text{var } a + \langle a \rangle \quad (13)$$

which will be very useful in the following.

Substituting the Poisson expansion (12) into the forward Kolmogorov equation (11) and after a few algebraic manipulations (see section 3 in the supporting information), we end up with a governing equation for $f(\mathbf{a}, t)$

$$\frac{\partial}{\partial t} f(\mathbf{a}, t) = \sum_i \mu_i \frac{\partial^2 a_i f}{\partial a_i^2} - \frac{\partial}{\partial a_i} \{ [\lambda_i - a_i(\sigma_i + \nu_i - \mu_i)] f \} + \frac{\partial}{\partial a_{i-1}} (\nu_{i-1} a_{i-1} f) \quad (14)$$

The main advantages of this transformation appear here clearly: we have reduced the degree of coupling between the equations and the resulting set of equations is a multivariate advection-diffusion equation that can be interpreted as a Fokker-Planck equation. Therefore, we can use the equivalence between Fokker-Planck equations and stochastic differential (Langevin) equations [Gardiner, 1983]. The *Langevin representation* equivalent to equation (14) is

$$da_i(t) = (\lambda_i - a_i(\sigma_i - \mu_i) + \nu_{i-1} a_{i-1} - \nu_i a_i) dt + \sqrt{2\mu_i a_i} dW_i(t) \quad (15)$$

which holds for $a_i \geq 0$ ($i = 2, 3, \dots$) and where W_i ($s^{1/2}$) is a Wiener process (white noise) for cell i . Under homogeneous conditions ($\lambda_i = \lambda$, $\sigma_i = \sigma$, and $\mu_i = \mu$ for $1 \leq i \leq M$), the mean steady state solution to the Langevin equation (15) is

$$\langle a \rangle_{ss} = \frac{\lambda}{\sigma - \mu} \quad (16)$$

It is now very tempting to take the continuum limit $\Delta x \rightarrow 0$ and introduce the *Poisson density* b (m^{-1}), particle activity γ (m), and ensemble-averaged particle activity c (m):

$$b(x_i, t) = \lim_{\Delta x \rightarrow 0} \frac{a_i(t)}{\Delta x}, \gamma(x_i, t) = \lim_{\Delta x \rightarrow 0} \frac{\varpi_p N_i(t)}{B \Delta x} \text{ and } c(x_i, t) = \langle \gamma \rangle \quad (17)$$

with x_i the center of cell i , B (m) the stream width, and ϖ_p (m^3) the particle volume. Table 1 recaps the different variables used and their relationships between the Poisson (probability) space and real world.

If a_i were a continuous variable, it would be also very tempting to interpret the difference $\nu_{i-1} a_{i-1} - \nu_i a_i$ as the gradient $-\partial_x(\bar{u}_p b)$ in the continuum limit $\Delta x \rightarrow 0$. If so, we should end up with a governing equation for b

$$\frac{\partial}{\partial t} b(x, t) + \frac{\partial}{\partial x} (\bar{u}_p b) = \tilde{\lambda} - (\sigma - \mu) b + \sqrt{2\mu b} \xi_b \quad (18)$$

where we introduce $\tilde{\lambda} = \lambda/\Delta x$ ($\text{m}^{-1} \text{s}^{-1}$) the entrainment rate per unit length and we define a Gaussian noise term $\xi_b(x, t)$ ($\text{m}^{-1/2} \text{s}^{-1/2}$) such that $\langle \xi_b(x, t)\xi_b(x', t') \rangle = \delta_x(x-x')\delta_t(t-t')$, i.e., a white noise term that is uncorrelated in time and space, and δ_x (m^{-1}) and δ_t (s^{-1}) are Kronecker's deltas (i.e., $\delta_t(t) = 0$ if $t \neq 0$, and 1 for $t = 0$). Within our framework, the white noise term $\xi_b(x, t)$ is a generalization of white noise, which satisfies

$$\lim_{\Delta x \rightarrow 0} \frac{dW_i(t)}{\sqrt{\Delta x}} = \xi_b(x, t)dt \quad (19)$$

This definition of $\xi_b(x, t)$ is essential to properly encoding the white noise term in the numerical simulations.

Making use of the relation (13) between the a and n moments and the rule $\langle \sqrt{2\mu b}\xi_b \rangle = 0$, we deduce that the ensemble average of equation (18) leads to a simple advection equation for the particle activity c

$$\frac{\partial}{\partial t}c(x, t) + \frac{\partial}{\partial x}(\bar{u}_p c) = s(c) \quad (20)$$

where $s(c) = \lambda' - (\sigma - \mu)c$ is the linear source term and $\lambda' = \varpi_p \tilde{\lambda}/B$ (ms^{-1}) is the volumetric entrainment rate. A caveat is in order here: the treatment of the colored noise term $\sqrt{2\mu b}\xi_b$ in equation (18) can be achieved following two different approaches [Gardiner, 1983]: in the Itô interpretation, the value of b is taken before the jump; an important consequence is that $\langle \sqrt{2\mu b}\xi_b \rangle = 0$. Another possibility is the Stratonovich interpretation, which takes the mean of b before and after the jump (and in that case $\langle \sqrt{2\mu b}\xi_b \rangle \neq 0$). The latter interpretation is often seen as the most natural choice from a physical standpoint [Ridolfi et al., 2011], but unfortunately it leads to substantial mathematical difficulties when trying to solve stochastic differential equations analytically. So, following the usage in the physics of reaction-diffusion problems [Gardiner, 1983], we have adopted the Itô convention. Comparing equations (1) and (20), we note that the advection terms are not strictly similar (except if the advection velocity does not depend on x): in the original advection-diffusion equation (1), the operator $\partial_t + \bar{u}_p \partial_x$ is the material derivative and represents the rate of change of particle activity observed by particles. Equation (20) is the conservative form of the advection-diffusion equation (1) and the advection term $\partial_x(\bar{u}_p c)$ represents the flux of particle activity through a vertical slice.

The statistical properties of c can be inferred from equations (18) and (13). Under homogeneous steady state conditions, we find (see section 4 in the supporting information) for the mean Poisson density, the spatial cross correlation, and variance

$$\langle b \rangle_{ss} = \frac{\tilde{\lambda}}{\sigma - \mu}, \quad \langle b(x)b(x+r) \rangle_{ss} = \langle b \rangle_{ss} \frac{\mu \delta_r(r) + \tilde{\lambda}}{\sigma - \mu} \quad \text{and} \quad \text{var}_{ss} b = \frac{\mu \tilde{\lambda}}{(\sigma - \mu)^2} \delta_r(0) \quad (21)$$

where $\delta_r(r)$ (m^{-1}) is Kronecker's delta and for the autocorrelation function

$$\rho(t) = \exp(-(\sigma - \mu)t) \quad (22)$$

Surprisingly, these properties are independent of the advection velocity \bar{u}_p . This may seem a priori plausible in that advection is just a mode of transport of particles, which under steady state conditions fades out. Note also that these properties are independent of the position and so they hold true for any x or over any control volume. It also follows that the analytical results obtained for one-cell systems ($M = 1$) should hold true here; in particular, the probability density function of a_i (under steady state conditions) should be the gamma distribution $Ga(\alpha, \beta)$ with parameters $\alpha = \lambda/\mu$ and $\beta = \mu/(\sigma - \mu)$ [Ancey and Heyman, 2014].

However, as shown just below (see section 3), numerical simulations of the Langevin equations (15) reveal that the story is a bit more complicated. They demonstrate that diffusion-like effects occur and thus, the link between the advection equation (20) (giving a picture of the system at the bulk scale) and the underlying Langevin equations (15) (describing the system at the microscale) is more subtle than what the derivation above suggests.

3. Numerical Tests

In the following, we will analyze the microscopic behavior in particular cases by solving the system of Langevin equations (15) and compare the results with the macroscopic features predicted by the continuum formulation (20) or the expected statistical properties (21).

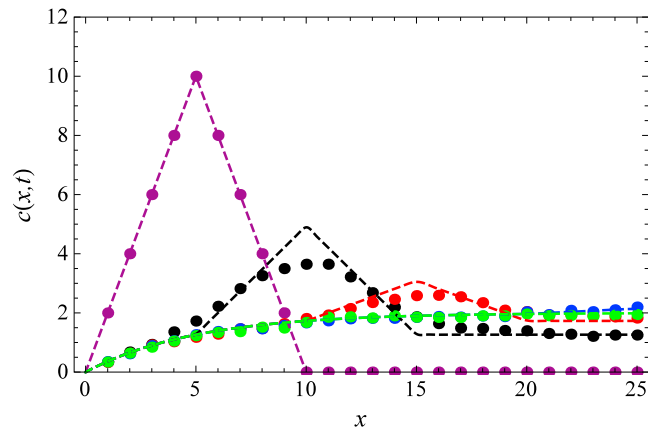


Figure 3. Example of simulation of the Langevin equations (15) with $\lambda = 2 \text{ s}^{-1}$, $\sigma = 5 \text{ s}^{-1}$, $\mu = 4 \text{ s}^{-1}$, and $v = 5 \text{ s}^{-1}$ ($D_* = 2.5 \text{ m s}^{-2}$). The dots represent the mean particle activity averaged over 500 samples obtained by solving equation (15) numerically using an Euler scheme [Iacus, 2008] with a time step $dt = 0.01 \text{ s}$. The dashed line shows the pure advection behavior of equation (20) at times $t = 0, 1, 2, 4, 8 \text{ s}$. The exact solution to equation (20) is provided in section 11 of the supporting information. The initial ($t = 0 \text{ s}$) conditions are shown in purple. The boundary conditions are $c = 0$. We show only the first 25 cells.

We solved the system of Langevin equations (15) numerically using an Euler scheme with time step $dt = 0.01 \text{ s}$ (see section 5 in the supporting information) [Higham, 2001; Iacus, 2008]. The computational domain was split into $M = 100$ cells of length $\Delta x = 1 \text{ m}$. The sample mean and variance, $\langle n \rangle$ and $\text{var } a$ for each cell were computed over 500 simulations. Note that making use of equations (13) and (17), we also find the relationship between c and $\langle N \rangle$

$$\langle c \rangle_{ss} = \frac{\overline{w}_p}{B\Delta x} \langle N \rangle_{ss} \text{ and } \text{var}_{ss} a = \Delta x^2 \text{var}_{ss} b \quad (23)$$

since the variance of b is found to be independent of x . The continuum formulation (20) is a simple hyperbolic partial differential equation that can be solved exactly using the method of characteristics (see section 11 in the supporting information).

3.1. Mean Behavior of the Particle Activity

Let us first consider a sharp gradient in the particle activity and let us see how this particle activity evolves with time when at the microscale, the particles are advected at constant velocity \bar{u}_p . Figure 3 shows the propagation of an initial pulse of sediment: the evolution of the initial (triangle-shaped) pulse is dictated by the displacement, deposition, and entrainment processes (5), (8), and (9). In the numerical simulations (dots) at $t = 1 \text{ s}$, the initial peak is rapidly smoothed out while on the right, the particle activity tends continuously to a constant value. This contrasts with the advection solution (dashed line), which conserves the initial shape, i.e., a peak and a sharp transition from the peak to the plateau. This simple example shows that the advection equation (20) captures the mean behavior fairly well, but it fails to provide the correct values in regions marked by a discontinuity in the particle activity gradient. This is an indication of nonlocal or diffusive effects, which smear out sharp variations in c .

3.2. Statistical Behavior of the Particle Activity

Another example is provided by the computation of the expected statistical features of the particle activity, here the mean and variance of a under steady state conditions. We use the relationship (13) relating the moments of N and a together with the definition of the particle activity (18). We solved an initial boundary value problem with the initial condition $a_i = 1$ for $1 \leq i \leq M$ (equivalently $c(x, 0) = 1$) and the following boundary condition on the left of the domain $a_0(t) = 0$ (ghost cell) for $t > 0$ (equivalently $c(0, t) = 0$). These two conditions are not strictly compatible initially at $x = 0$; we imposed a nonzero initial state to preclude generating negative a_i values in the initial steps. Figure 4 shows numerical simulations of this initial boundary value problem. As expected, the process $a_i(t)$ tends toward the steady state value $\langle a \rangle_{ss} = \lambda / (\sigma - \mu) = 10$ given by equation (16): Figures 4a and 4c show that both the spatial and the time variation of the process $a_i(t)$ are well captured by the analytical solution to the advection equation (20). Under steady state conditions, the values $a_i(t)$ fluctuate randomly around the mean steady state value, but the computed sample variance is much

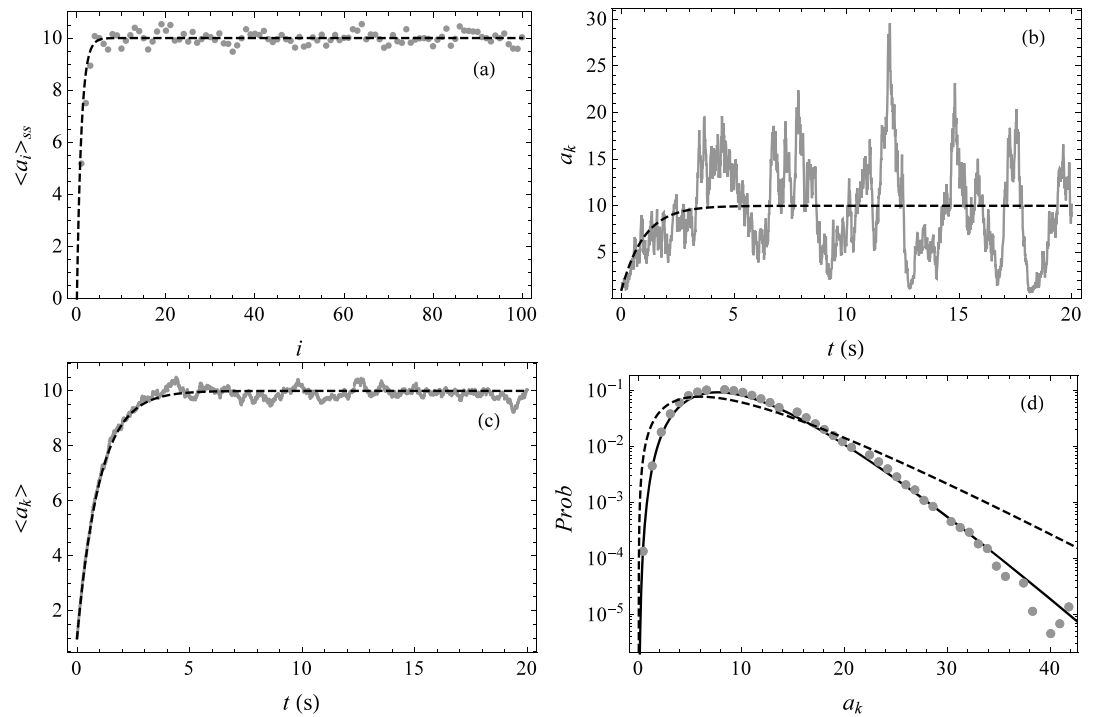


Figure 4. Example of simulation of equation (15) with $\lambda = 10 \text{ s}^{-1}$, $\sigma = 5 \text{ s}^{-1}$, $\mu = 4 \text{ s}^{-1}$, $\nu = 1 \text{ s}^{-1}$. (a) Variation of $\langle a_i \rangle$ as a function of the position i ($1 \leq i \leq M$) at time $t = 20$ s. (b) Particular realization of the process $a_k(t)$ for $k = 50$ (middle of the computational domain). (c) Time variation of $\langle a_k(t) \rangle$ for $k = 50$. (d) Probability distribution function of a_k for $k = 50$; the solid line is the gamma distribution $Ga(\tilde{\alpha}, \tilde{\beta})$, whose parameters have been calculated using the mean and variance obtained iteratively in section 3.3 (approximation of $\text{var}_{ss} a / \langle a \rangle$ to order $K = 20$). The dots represent the simulated values a_i . Averages and probabilities were computed over 500 samples once steady state has been reached (in practice for $t \geq 10$ s). For Figures 4a to 4d, the dots and gray lines show the numerical simulations. For Figures 4a to 4c the dashed line shows the pure advection behavior obtained by solving the advection equation (20) using the method of characteristics (see section 11 of the supporting information) and employing equation (23); for Figure 4d, it is the gamma distribution $Ga(\alpha, \beta)$ with parameters $\alpha = \lambda/\mu$ and $\beta = \mu/(\sigma - \mu)$.

lower than the theoretical value given by equation (21): for instance, for cell $k = 50$, we found $\text{var}_{ss} a_k = 23.19$ in our simulations, whereas the theoretical value is 40. A closer look at the empirical probability distribution (see Figure 4d) reveals that the theoretical gamma distribution $Ga(\alpha, \beta)$ roughly describes the empirical probabilities. The difference is especially visible in the tail of the distribution (for $a_k > 20$), for which theory overestimates the probabilities significantly. Figure 5 shows the empirical autocorrelation function and its theoretical expression (22). Theory clearly overestimates the autocorrelation.

As a summary, we have found that the mean behavior is closely described by the advection equation (20): the steady state and the transient to this regime are fairly well described, but deviations from the simulated behavior are seen in regions characterized by sharp transitions in the particle activity. Moreover, there is clear evidence that the theoretical statistical properties (here variance and autocorrelation) are poorly estimated by equation (21).

Simulations were performed for other sets of values λ , σ , μ , and ν , and we systematically observed that theory goes right with the prediction of the mean behavior in the absence of sharp variations in c and goes awry in the estimation of the statistical properties. Figure 6 shows how the sample variance varies with the emigration rate ν : there is a clear drop in the variance $\text{var}_{ss} a$ with ν , which is visible for ν values as low as $\nu = 0.1 \text{ s}^{-1}$. For $\nu = 1 \text{ s}^{-1}$, there is a factor of 2 between theory and simulation and for $\nu = 10 \text{ s}^{-1}$, this factor exceeds 4.

3.3. Analysis

To understand the origin of the discrepancy between theory and simulations, we need to return to the original Langevin equations (15), which are the fundamental equations from which we derived the continuum version (18). If we ignore the noise term in equation (15), we note that they also bear close resemblance to the discretized equations obtained from finite-difference (upwind scheme) and finite-volume methods used

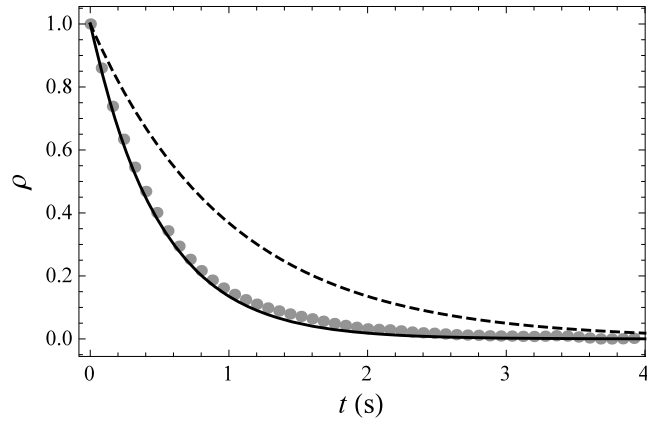


Figure 5. Autocorrelation function for cell $k = 50$ (averaged over 500 samples once the steady state has been reached) with $\lambda = 10 \text{ s}^{-1}$, $\sigma = 5 \text{ s}^{-1}$, $\mu = 4 \text{ s}^{-1}$, and $\nu = 1 \text{ s}^{-1}$. The dots represent the empirical autocorrelation function. The dashed line shows the pure advection behavior given by equation (22). The solid line represents the first-order correction given by (33).

for solving the deterministic advection equation [LeVeque, 2002], and we will use this analogy to interpret the observed discrepancy (see section 3.4).

We start with the calculation of the second-order moment for cell i

$$\frac{d}{dt} \langle a_i^2 \rangle = 2\lambda \langle a_i \rangle - 2(\sigma + \nu - \mu) \langle a_i^2 \rangle + 2\nu \langle a_i a_{i-1} \rangle + 2\mu \langle a_i \rangle \quad (24)$$

where we have made use of the Itô rule for calculating da_i^2 from da_i [Gardiner, 1983]. This equation involves the unknown cross correlation $\langle a_i a_{i-1} \rangle$. Assuming that a homogeneous steady state regime has been reached, we have $\lambda \langle a_i \rangle_{ss} = \lambda \langle a \rangle_{ss}$ for any cell i , we then obtain for the second-order moment

$$2(\sigma + \nu - \mu) \langle a^2 \rangle_{ss} = 2\lambda \langle a \rangle_{ss} + 2\nu \langle a_i a_{i-1} \rangle_{ss} + 2\mu \langle a \rangle_{ss} \quad (25)$$

We need to calculate $\langle a_i a_{i-1} \rangle_{ss}$. This is readily done by multiplying equation (15) by a_{i-1} and by doing the same for this equation applied to cell $i - 1$. An equation for the cross correlation $\langle a_i a_{i-1} \rangle$ is then obtained

$$\frac{d}{dt} \langle a_i a_{i-1} \rangle = \lambda (\langle a_i \rangle + \langle a_{i-1} \rangle) - 2(\sigma + \nu - \mu) \langle a_i a_{i-1} \rangle + \nu \langle a_{i-1}^2 \rangle + \nu \langle a_i a_{i-2} \rangle \quad (26)$$

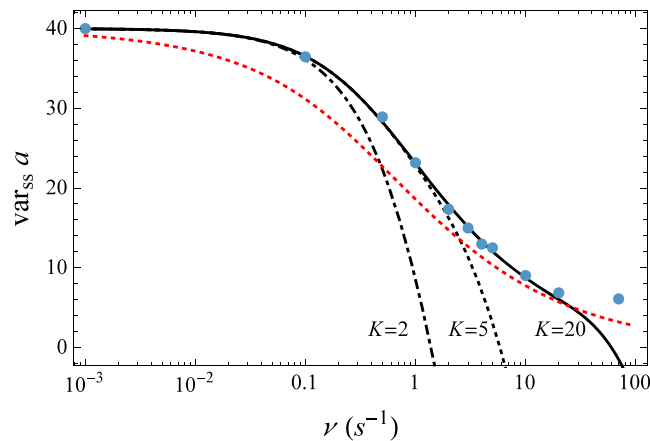


Figure 6. Steady state variance $\text{var}_{ss} a$ as a function of the emigration rate ν . The dots show the numerical simulations with $\lambda = 10 \text{ s}^{-1}$, $\sigma = 5 \text{ s}^{-1}$, and $\mu = 4 \text{ s}^{-1}$. The dash-dotted line, dotted line, and solid line represent the variance to order $K = 2, 5,$ and 20 , respectively, calculated iteratively from the cross correlations $\langle a_i a_{i-k} \rangle$ (see section 6 in the supporting information for further detail). The red dotted line is the variance given by equation (37) for a purely diffusive process with $D_* = \nu \Delta x^2 / 2$.

which under steady state conditions gives

$$2(\sigma - \mu + \nu)\langle a_i a_{i-1} \rangle_{ss} = 2\lambda \langle a \rangle_{ss} + \nu \langle a^2 \rangle_{ss} + \nu \langle a_i a_{i-2} \rangle_{ss} \quad (27)$$

which depends on $\langle a_i a_{i-2} \rangle_{ss}$. Repeating the procedure for $\langle a_i a_{i-2} \rangle_{ss}$ and longer-range terms, we end up with a hierarchy of coupled equations for the spatial cross correlations.

To close the system to order 2, let us assume that the last term $\nu \langle a_i a_{i-2} \rangle_{ss}$ in equation (27) is zero, then

$$\langle a_i a_{i-1} \rangle_{ss} = \frac{\lambda}{\sigma + \nu - \mu} \langle a \rangle_{ss} + \frac{\nu}{2(\sigma + \nu - \mu)} \langle a^2 \rangle_{ss} \quad (28)$$

and after substitution into equation (25), we get

$$2(\sigma + \nu - \mu) \langle a^2 \rangle_{ss} = 2(\lambda + \mu) \langle a \rangle_{ss} + 2\nu \left(\frac{\lambda}{\sigma + \nu - \mu} \langle a \rangle_{ss} + \frac{\nu}{2(\sigma + \nu - \mu)} \langle a^2 \rangle_{ss} \right)$$

from which we deduce the following approximation of the variance for $\nu \ll 1$

$$\text{var}_{ss} a = \frac{\lambda \mu}{(\sigma + \nu - \mu)^2} \left(1 + \frac{\nu}{\sigma + \nu - \mu} + \frac{1}{2} \left(3 - \frac{\lambda}{\mu} \right) \frac{\nu^2}{(\sigma + \nu - \mu)^2} + O(\nu^2) \right) \quad (29)$$

which depends on ν and gives equation (21) in the limit $\nu \rightarrow 0$ (when dividing it by Δx^2). Higher-order approximations can be obtained iteratively by calculating the correlations $\langle a_i a_{i-k} \rangle_{ss}$ in the same way and closing the system by assuming that at order K , the last correlation term $\langle a_i a_{i-K-1} \rangle_{ss}$ is zero (see section 6 in the supporting information). Figure 6 shows the variance calculated iteratively to order $K = 2, 5$, and 20. High-order expansions are needed to match the numerical simulations for $\nu > 0.1 \text{ s}^{-1}$. For instance, for $\nu = 1 \text{ s}^{-1}$, we found numerically that $\text{var}_{ss} a = 23.19$. With $K = 2$ (given by the approximation (29)), 5, and 20, we found $\text{var}_{ss} a = 8.57, 22.81, 23.09$, respectively.

If now we use the value of the variance obtained by this iterative procedure, we can update the parameters of the gamma distribution ($\tilde{\alpha} = \langle a \rangle_{ss}^2 / \text{var}_{ss} a$ and $\tilde{\beta} = \text{var}_{ss} a / \langle a \rangle_{ss}$) and plot the corresponding probability distribution function. Figure 6 shows that the updated theoretical distribution compares well with the numerical data. The slight deviations seen in the tail (for $a_k > 35$) result from the low number of extreme values in the numerical simulations. The good agreement between the theoretical curve and numerical data demonstrates that the advection velocity does not affect the type of the distribution but merely the variance $\text{var}_{ss} a$.

The calculations show that in contrast with theoretical predictions, the variance of the simulated samples decreases with increasing ν because the cross correlation exhibits a longer-range dependence than theory predicts. This introduces *nonlocal* effects, which take the appearance of diffusion. This is why the emigration rate ν affects the statistical properties of the particle activity in contrast with the theoretical predictions (21).

In the sediment transport literature, the concept of nonlocal effects is used to describe situations in which the particle flux in a given place depends not only on local conditions but also on hillslope conditions far upstream or downstream of the point of measurement [Furbish and Roering, 2013]. For models based on random walks, nonlocality is often associated with large jumps of the particles (relative to the size of the system) or correlation of velocities [Tucker and Bradley, 2010]. Here nonlocality arises because the spatial cross correlations are nonzero (see below) and the calculation of the local variance (in cell i) requires the knowledge of the spatial cross correlations over a significant distance from cell i (depending on the emigration rate ν), whereas for a genuinely local advection process in a steady state, these spatial cross correlations should vanish. Another way of looking at the issue of nonlocality is to express the mean Poisson rate $\langle a_i \rangle$ as a convolution sum. Assuming that the system reaches a steady (but not necessarily homogeneous) state and taking the ensemble average of the Langevin equations (15), we can recast the latter system of equations in matrix form

$$\mathbf{A} \cdot \langle \mathbf{a} \rangle = \mathbf{\Lambda} \quad (30)$$

where $\mathbf{\Lambda}$ is the column vector $(\lambda_i)_{1 \leq i \leq M}$ and \mathbf{A} is an $M \times M$ lower bidiagonal matrix, whose main diagonal elements are $\sigma_i - \mu_i + \nu_i$ ($1 \leq i \leq M$) and the lower diagonal entries are $-\nu_{i-1}$ ($2 \leq i \leq M$) (all other entries are zero). The inverse of a lower bidiagonal matrix is a lower triangular matrix \mathbf{L} , whose entries can be calculated exactly (see section 12 in the supporting information). So we deduce that

$$\langle \mathbf{a} \rangle = \mathbf{L} \cdot \mathbf{\Lambda} \quad (31)$$

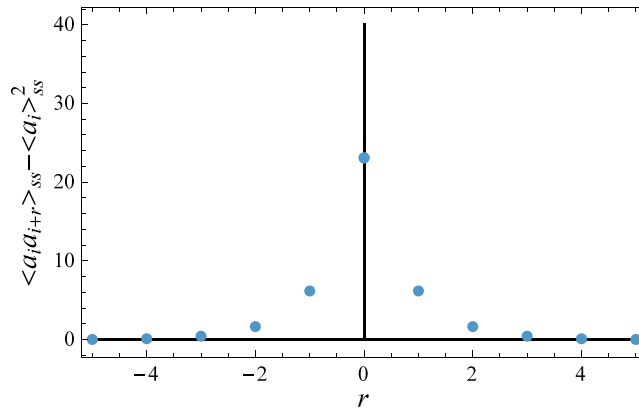


Figure 7. Covariance (spatial cross correlations) $\langle a_i a_{i+r} \rangle_{ss} - \langle a_i \rangle_{ss}^2$ for the Langevin equations (15) (dots) under steady state conditions, with $\lambda = 10 \text{ s}^{-1}$, $\sigma = 5 \text{ s}^{-1}$, $\mu = 4 \text{ s}^{-1}$, $\nu = 1 \text{ s}^{-1}$, and for the process $b(x, t)$ given by equation (21) (solid line).

or said differently, this means that the Poisson rate at cell i depends on what happens upstream of it

$$\langle a_i \rangle = \sum_{k=1}^i L_{ij} \lambda_j \text{ for } 1 \leq i \leq M \quad (32)$$

Similar iterative calculations can be made with the autocorrelation function (see section 7 in the supporting information) and to first order, we find

$$\rho(t) = \exp(-(\sigma + \nu - \mu)t), \quad (33)$$

which introduces a dependence on ν . Note that this autocorrelation function is the same as the one found in one-cell systems [Ancey *et al.*, 2008]. Figure 5 compares the approximate and empirical autocorrelation functions for ν and shows a fairly good agreement between both, confirming the effect of ν on the autocorrelation time: the higher the emigration rate, the shorter the autocorrelation time $t_c = (\sigma + \nu - \mu)^{-1}$.

As a summary, the analysis of the Langevin equations (15) shows that the common assumption $(\nu_i a_i - \nu_{i-1} a_{i-1})/\Delta x \rightarrow \partial_x(\bar{u}_p b)$ —used above in the derivation of equation (18)—is valid only when $\Delta x \rightarrow 0$. For finite lengths Δx (a case that is mostly encountered whenever we perform laboratory experiments or numerical simulations using discretized equations), the approximation $\partial_x(\bar{u}_p b) \approx (\nu_i a_i - \nu_{i-1} a_{i-1})/\Delta x$ is incorrect. The essential difference with deterministic motion is that a_i fluctuates randomly and so does the difference $a_{i-1} - a_i$, which means that even under steady state conditions (zero gradient on average), there is particle transport due to local fluctuations of particle activity. As shown by Figure 7, the analysis of the spatial covariance shows that the covariance $\langle a_i a_{i+r} \rangle_{ss} - \langle a_i \rangle_{ss}^2$ is non zero for neighboring cells (up to $|r| = 2$), whereas theory predicts a zero covariance (see equation (21)). Fluctuations attenuate the peak of covariance at $r = 0$ (i.e., the variance $\text{var}_{ss} a$) but exacerbate correlations between neighboring particles. This also explains why diffusion-like effects occur when there are sharp gradients in the particle activity (see Figure 3).

The moral of the story is that for a finite cell size Δx , using birth-death Markov processes is quite useful for describing the local behavior of particles, but taking the ensemble average does not lead exactly to the desired advection equation for the particle activity. Slight deviations between the actual and predicted particle activities may occur as a result of finite spatial correlations between neighboring particles that produce diffusion-like spreading of particles. This behavior brings to mind the recent findings by Furbish and Roering [2013]: these authors defined the particle flux in the form of a convolution integral involving the distribution of particle travel distances and mobilization rates at all upslope positions (this is the hallmark of nonlocal transport). Next, they demonstrated that under certain conditions (the first two moments of the travel distance distribution must be finite), this particle flux can also be recast in the form of an advection-diffusion equation, giving the appearance of local behavior. Similarly, we find that the apparently diffusive effect reflects a nonlocal process (nonzero spatial correlation, expression of a_i as a convolution sum). Even though diffusion is absent from the original process in equation (15), the nonlocal properties can be approximated by a local diffusion operator. The mean behavior is slightly disturbed by this effect, but the statistical properties of particle activity (analyzed through the Poisson density b) are profoundly affected.

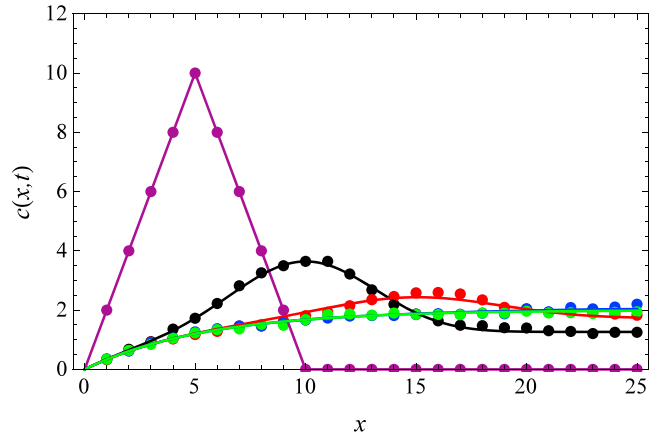


Figure 8. Example of simulation of the Langevin equations (15) with $\lambda = 2 \text{ s}^{-1}$, $\sigma = 5 \text{ s}^{-1}$, $\mu = 4 \text{ s}^{-1}$, and $\nu = 5 \text{ s}^{-1}$ ($D_* = 2.5 \text{ m s}^{-2}$). The dots represent the mean activity averaged over 500 samples obtained by solving equation (15) numerically. The solid line shows the advective diffusive behavior predicted by equation (36) at times $t = 0, 1, 2, 4$, and 8 s . Same conditions as for Figure 3.

3.4. Approximation of the Diffusive Behavior

We have seen that nonlocal effects occur in the advection of particles at constant velocity and that these effects look like diffusion. The idea developed here is to interpret the difference $v_i a_i - v_{i-1} a_{i-1}$ as transport and diffusion but with a diffusivity coefficient that depends on the cell length Δx . In this way, if we are only interested in the mean behavior, we can mimic the results obtained by solving the Langevin equations (15) using deterministic partial differential equations such as equation (20). To this end, we will draw an analogy with the numerical diffusion introduced by upwind methods when solving advection equations numerically [e.g., see *LeVeque, 2002*, section 8.6.1].

The idea is to introduce a central difference scheme. Let us break down the difference $v_{i-1} a_{i-1} - v_i a_i$ as follows

$$(v_i a_i - v_{i-1} a_{i-1}) = \frac{1}{2}(v_{i+1} a_{i+1} - v_{i-1} a_{i-1}) - \frac{\Delta x^2}{2} \frac{v_{i+1} a_{i+1} + v_{i-1} a_{i-1} - 2v_i a_i}{\Delta x^2} \quad (34)$$

According to the classical decomposition used in finite-difference methods, this equation can be interpreted as follows: the first term on the right-hand side represents advection at rate ν , which is modulated by the second contribution representing diffusion at rate $D_* = \nu \Delta x^2 / 2 = \bar{u}_p \Delta x / 2$. This scheme is known to lead to unstable schemes for deterministic problems with $s = 0$ [*LeVeque, 2002*], but here we will show that it mimics the diffusive effects induced by noise transmission from cell to cell and furthermore, from the numerical point of view, it is conditionally stable (see section 8 in the supporting information).

Making use of the decomposition (34), we find that the continuum equivalent of the Langevin equations (15) is a stochastic partial differential equation

$$\frac{\partial}{\partial t} b(x, t) + \frac{\partial}{\partial x} (\bar{u}_p b) = \frac{\partial^2}{\partial x^2} (D_* b) + \tilde{\lambda} - (\sigma - \mu) b + \sqrt{2\mu} b \xi_b \quad (35)$$

Now taking the ensemble average of equation (35) leads to the evolution for $c(x, t)$ in the form of an advection-diffusion equation

$$\frac{\partial}{\partial t} c(x, t) + \frac{\partial}{\partial x} (\bar{u}_p c) = s(c) + \frac{\partial^2}{\partial x^2} (D_* c) \quad (36)$$

with $s(c) = \lambda' - (\sigma - \mu)c$. Here we touch a sore point of this approximation. In the classical advection-diffusion equation (1), the diffusivity does not depend on the spatial scale, whereas here D_* depends on the cell (mesh) size Δx . Rigorously, for $\Delta x \rightarrow 0$, we have $D_* \rightarrow 0$ since \bar{u}_p remains finite. So this approximation is just an expedient to mimic the expected mean behavior for c .

As an example, we consider the spreading of an initial pulse of sediment, which has been studied in Figure 3. Figure 8 shows the same data as shown in Figure 3 and the numerical solution to the advection-diffusion equation (36) (obtained using the method of lines and Adam-Moulton technique). This solution captures well

the particle activity behavior at different times, confirming the occurrence of the diffusion-like effects in the Langevin equations (15) where there are sharp activity gradients. We also tested the capacity of the underlying Langevin equation (35) to predict the statistical properties of particle activity. For instance, it can be shown (see section 9 in the supporting information) that for processes affected by diffusion, the sample variance for a cell of length Δx is

$$\text{var } a = \frac{\mu \lambda}{\kappa^2} \frac{\ell_c}{\Delta x^2} \left(\frac{\Delta x}{\ell_c} + \exp\left(-\frac{\Delta x}{\ell_c}\right) - 1 \right) \quad (37)$$

with $\ell_c = \sqrt{D_*/(\sigma - \mu)}$ the correlation length. Figure 6 shows the sample variance $\text{var}_{ss} a$ as a function of v . There is clearly a significant decrease in $\text{var}_{ss} a$ with increasing v . The theoretical curve (37) including space-dependent diffusion roughly captures the data and so can be used as a first approximation of the sample variance.

4. Inclusion of Particle Velocity Fluctuations

As highlighted in section 1, much of the attention in the literature has been paid to diffusion-reaction equations and in that particular case, there are sound results showing how diffusion-reaction equations (equation (1) with $\bar{u}_p = 0$) can be derived within the framework of birth-death Markov processes [Gardiner, 1983; Gillespie and Seitaridou, 2013]. Concerning sediment transport, we have recently shown that under flow conditions that are very commonly encountered, particle motion can be broken down into advection and diffusion. In that case, diffusion refers to the spreading of particles arising from the velocity fluctuations (i.e., the differences between the mean velocity \bar{u}_p and their instantaneous velocity u_s) [Ancey and Heyman, 2014]. There is an ongoing debate about the probability distribution of the particle velocities, with at least two distinctive results: exponential distribution [Lajeunesse et al., 2010; Furbish and Schmeeckle, 2013; Fan et al., 2014] and Gaussian-like distribution [Martin et al., 2012; Ancey and Heyman, 2014]. Regardless of the actual distribution for u_s , it can be shown that particle diffusion is the limit of a local jump process, i.e., particles can be transferred from one cell i to its neighboring cells $i - 1$ or $i + 1$ with probabilities, respectively,

$$p_i^4 = \text{Prob}(\mathbf{N} = \mathbf{n} + \mathbf{r}_i^{j-1}; t + \delta t) = d_i N_i \delta t \quad (38)$$

and

$$p_i^5 = \text{Prob}(\mathbf{N} = \mathbf{n} + \mathbf{r}_i^{j+1}; t + \delta t) = d_i N_i \delta t \quad (39)$$

where d_i is the local diffusion rate. The forward Kolmogorov equation (11) must then be updated. The reader is referred to Ancey and Heyman [2014] for the detail. Making use of the Poisson representation, we have shown that this updated forward Kolmogorov equation (11) is equivalent to the Langevin equations

$$da_i(t) = (\lambda_i - a_i(\sigma_i - \mu_i) + v_{i-1}a_{i-1} - v_i a_i + d_i(a_{i+1} + a_{i-1} - 2a_i)) dt + \sqrt{2\mu_i a_i} dW_i(t) \quad (40)$$

which are similar to equation (15) apart from the terms $d_i(a_{i+1} + a_{i-1} - 2a_i)$. If we define the (bulk) diffusivity D as

$$D = \lim_{\Delta x \rightarrow 0} \Delta x^2 d_i \quad (41)$$

then the continuum version of these new Langevin equations when $\Delta x \rightarrow 0$ is

$$\frac{\partial}{\partial t} b(x, t) + \frac{\partial}{\partial x} (\bar{u}_p b) = s(b) + \frac{\partial^2}{\partial x^2} (Db) + \sqrt{2\mu b} \xi_b \quad (42)$$

We deduce that the ensemble average of equation (42) leads to an advection-diffusion equation for the particle activity c

$$\frac{\partial}{\partial t} c(x, t) + \frac{\partial}{\partial x} (\bar{u}_p c) = s(c) + \frac{\partial^2}{\partial x^2} (Dc) \quad (43)$$

which is very close to the classical form equation (1). The statistical properties of the Langevin equations (42) have been investigated in our earlier papers [Ancey and Heyman, 2014]. For a homogeneous steady state, we have found for the mean value, the covariance, and the variance

$$\langle b \rangle_{ss} = \frac{\tilde{\lambda}}{\sigma - \mu}, \text{cov}_{ss} b(r) = \frac{1}{2} \frac{\mu}{\sigma - \mu} \frac{\langle b \rangle_{ss}}{\ell_c} \exp^{-r/\ell_c}, \text{ and } \text{var}_{ss} b = \frac{1}{2} \frac{\mu}{\sigma - \mu} \frac{\langle b \rangle_{ss}}{\ell_c} \quad (44)$$

with $\ell_c = \sqrt{D/(\sigma - \mu)}$ the correlation length. Again, we can express surprise as these properties are unaffected by the advection velocity. Numerical simulations of the Langevin equations (40) (see section 10 in the supporting information) lead to the same observations as for pure advection: the mean behavior is fairly well described, but the statistical properties (variance and autocorrelation time) are poorly estimated by equation (44).

5. Concluding Remarks

An essential question for all modelers is the choice of the governing equations and the scale of representation. In morphodynamic models, the use of phenomenological equations such as the Meyer-Peter and Müller equation has long been the common choice for modeling bed load transport. The key problem is that sediment transport exhibits considerable spatial and temporal fluctuations, whereas morphodynamic models predict mean behaviors for water, bed, and sediment transport. This makes the direct comparison between theory and observation quite difficult in practice [Recking *et al.*, 2012]. These models are also less successful at providing relevant responses to key issues such as bed form formation [Balmforth and Provenzale, 2001]. This failure has often been seen as the lack of physical details in the governing equations [Seminara, 2010]. For the water phase, models of greater complexity are now commonly used, e.g., two- or three-dimensional Reynolds equations with simple closure equations for turbulence [Wu, 2007]. For sediment transport and bed dynamics, how to develop more realistic models while keeping a reasonable level of complexity remains a challenge [Paola, 2011]. In this respect, we are firmly convinced that the theory of birth-death Markov processes offers a convenient framework for describing the dynamics of sediment transport. Its main strength lies in its proximity to the fundamental principles of mechanics: we define control volumes and perform mass balances over them. In the strict limit $\Delta x \rightarrow 0$, we are able to formally derive an advection-diffusion equation for c —equation (43)—that is fairly close to the classic form (1).

In this paper, we take a stab at modeling the dynamics of sediment transport, but we do not aim to describe its full complexity. To render the problem of microscopic description tractable, we used the following working assumptions: (i) we considered particles of the same size (so there is neither grain sorting nor bed armoring, two processes that are known to play an important part in sediment transport), (ii) we do not distinguish between saltating and rolling particles (whereas there is evidence that particle velocity depends significantly on the type of movement), (iii) particle activity is the key random variable that controls the strength of fluctuations of particle transport rate and bed elevation, and (iv) transport rates are sufficiently low for the birth-death framework to be relevant (if many events occur within a short time span, then this framework cannot be applied).

While the treatment of the diffusion term on the microscale and macroscale is well-established, we have seen with the stochastic numerical simulations of section 3 that for finite cell sizes Δx , the advection term introduces diffusion-like effects. The important consequence is that in most practical applications, for which we work with finite values of Δx , the actual observed diffusion of particles \hat{D} is slightly higher than the intrinsic particle diffusivity D :

$$\hat{D} = D + D_* = D \left(1 + \frac{1}{2} Pe \right) \quad (45)$$

with $D_* \approx \bar{u}_p \Delta x / 2$ and $Pe = \bar{u}_p \Delta x / D$ is the Péclet number. Depending on Péclet number (i.e., the respective values of D , Δx , and \bar{u}_p), the difference between the observed and intrinsic diffusivities may be quite significant and lead to errors in the calculation of the statistical properties of particle activity. Our numerical simulations show that this “trick” is sufficient to provide more realistic predictions of the sample variance and autocorrelation function (see section 10 of the supporting information) for $Pe \geq 2$. For $Pe < 2$, the use of the intrinsic diffusivity alone is sufficient to provide correct estimates of the variance (or other moments) and autocorrelation function.

We have also illustrated with examples that the error created in using the advection-diffusion equation (1) for computing mean particle activity is small except in regions marked by sharp variations in the particle activity or activity gradients. Similar observations were made with the stochastic Burgers equation, a nonlinear equation that is close to the advection-diffusion equation (1) and in which particle activity is replaced by velocity: the solution to which the scheme converges depends on the mesh size [Hairer and Voss, 2011] and velocity discontinuities are smoothed out even in the absence of diffusive terms [Audusse *et al.*, 2015]. This peculiar

behavior of stochastic advection seems to be a common feature of stochastic partial differential equations (as the topic is quite recent, we may miss the broader view). We have also shown that the diffusion-like effect reflects a nonlocal transport behavior (see section 3.3). Similarly to the recent findings by *Furbish and Roering* [2013], we have found that this nonlocal behavior can be closely approximated by scale-dependent diffusion, i.e., a mathematical operator related to local conditions.

As a last remark, we would like to emphasize that the comparative advantages of birth-death Markov processes over other microscopic approaches lie in the possibility of deriving simple continuum equations that represent the mean behavior at the macroscale and the availability of numerical techniques to solve the forward Kolmogorov equation (11) or its Poisson representations (15) and (40). Sediment transport is discrete by nature, but it is highly desirable that continuum equations are made available to keep the computational cost of numerical simulations as low as possible to facilitate their incorporation into morphodynamics models. The most recent random walk models lead to anomalous advection-diffusion equations involving fractional derivative operators [*Schumer et al.*, 2009; *Ganti et al.*, 2010; *Zhang et al.*, 2012; *Sun et al.*, 2015], for which numerical techniques are much more complicated than those used for solving the advection-diffusion equation (1). Discrete particle models and automaton models have attracted growing attention in recent years [*Narteau et al.*, 2009; *Tucker and Bradley*, 2010; *Hodge and Hoey*, 2012; *Gabet and Mendoza*, 2012]. While their numerical implementation is simple, there is no technique for deriving continuum equations from the rules used to describe particle behavior in this environment.

Appendix A: Experimental Conditions

The data presented in Figure 1 were presented in an earlier publication [*Heyman et al.*, 2014]. The time series data along with a Mathematica notebook for computing the particle transport rate and visualizing the time series can be obtained from the following data repository <http://dx.doi.org/10.6084/m9.figshare.1480646>. Further information on the experimental facility can be found in two PhD theses [*Mettra*, 2014; *Heyman*, 2014] (available from <http://http://library.epfl.ch/theses/>).

The flume was 2.5 m long and 8 cm wide. The mean streambed inclination θ was 7% (4.0°), but the mean bed slope varied between 6% and 8.4% over time due to bed form development. The water flow depth was $h = 1.37$ cm on average, leading to a depth-averaged water velocity $u = 53$ cm s^{-1} . The sediment was made of gravel with mean diameter $d_{50} = 6.25$ mm ($d_{30} = 6.0$ mm and $d_{50} = 6.8$ mm) and density $\rho_p = 2690$ kg m^{-3} . The flume was supplied with gravel at a constant feeding rate $q_s = 0.37$ pps (about 0.12 gs^{-1}).

The resulting Shields number was $Sh = \rho_w h \sin \theta / ((\rho_p - \rho) d_{50}) = 0.09$ ($\rho_w = 10^3$ kg m^{-3} the water density), the Froude number $Fr = u / \sqrt{gh} = 1.44$, the flow Reynolds number $Re = uWh / (W + 2h) / \nu_w = 5400$ ($W = 8$ cm the channel width, $\nu_w = 10^{-6}$ $\text{m}^2 \text{s}^{-1}$ the kinematic viscosity of water), the boundary Reynolds number $Re' = u_* h / \nu_w = 605$ ($u_* = \sqrt{gh \sin \theta}$ the shear velocity). We deduce that the flow is fully turbulent and supercritical. Additional experiments have shown that the critical Shields number (threshold for incipient motion) determined by visual inspection should be slightly lower than 0.07 [*Mettra*, 2014]. The Shields diagram gives an upper bound for the critical Shields number Sh_c close to 0.06 [*Buffington*, 1999] for $Re' \approx 600$. If we take this value, the transport stage is $T = Sh / Sh_c - 1 = 0.5$ and so we are just above the threshold of incipient motion. Note that the relative submergence $h / d_{50} = 2.2$ is low (very shallow flow).

Upon leaving the channel, each particle hits a metallic plate and the impact is recorded by a small accelerometer operated at 20,000 Hz and tied to the plate. A peak-over-threshold method is then applied to detect the times of consecutive particle impacts [*Mettra*, 2014]. If sufficient damping is provided to avoid spurious vibrations of the plate, this method ensures excellent time resolution in passage detection. As the grain size distribution is narrow, little error is made when converting the number of particles per unit time to a (volumetric) sediment transport rate. The same measurement system is used at the flume inlet to measure the incoming sediment transport rate.

Using the accelerometer, we record the arrival time of particles at the flume outlet. We count the number $n(t)$ of particles hitting the plate at the outlet between times t and $t + \Delta t$ (with $\Delta t = 60$ s the sampling time) and define the sediment transport rate as

$$q_s(t) = \frac{n(t)}{\Delta t}. \quad (\text{A1})$$

The experiment was run for 50 h. As the experiment started with a flat bed, a near-equilibrium state was observed after a few hours (once the mean streambed slope was adjusted and bed forms developed). The raw data included 67,972 events. We decided to keep the last 60,000 events. Said differently, the time series shown in Figure 1 corresponds to data acquired for times $t > 8.73$ h after the experiment started. The number of events was selected somewhat arbitrarily: we knew that the effects of the initial conditions (flat bed) must be dissipated before the system reached a near-equilibrium state, but as this state was poorly constrained (as shown by Figure 1), we had limited capacity to determine when the system reached steady state by merely looking at the time series $q_s(t)$. Monitoring the mean streambed slope (averaged over the flume length) in parallel with $q_s(t)$ revealed that it took approximately 6 h for this slope to converge to its steady state [Mettra, 2014].

Notation

Here we provide the list of variables used in the paper, their meaning, physical units, and the reference to the equations or sections, in which they were introduced.

Variable Meaning

a, \mathbf{a}	Poisson rate.
a_i	Poisson rate for cell i , equation (12).
b	Poisson density (m^{-1}) equation (16).
B	flume width (m).
c	mean particle activity (m).
D	particle diffusivity (ms^{-2}).
d_i	local diffusion rate ($\text{m}^{-1} \text{s}^{-2}$), equation (36).
D_*	fake diffusivity (ms^{-2}), equation (40).
D	deposition rate per unit area (s^{-1}), equation (7).
\mathcal{E}	entrainment rate per unit area (s^{-1}), equation (6).
f	probability density function in the a space.
g	gravity acceleration $g = 9.81 \text{ ms}^{-2}$.
ℓ_c	correlation length (m), equation (39).
N	number of moving particles within the window.
$\langle N \rangle$	mean number of particles within the window.
P	probability density function.
Pe	Péclet number $Pe = \bar{u}_p \Delta x / D$.
\bar{q}_s	time-averaged particle sediment rate (pps).
q_s	instantaneous particle sediment rate (pps).
\mathbf{r}	position vector (m).
t	time (s).
τ_c	autocorrelation time (s).
\bar{u}_p	mean particle (advection) velocity in ms^{-1} .
W	Wiener process ($\text{s}^{1/2}$).
W_i	local Wiener process ($\text{s}^{1/2}$), equation (15).
x	streamwise coordinate (m).
$\delta_r, \delta_t, \delta_x$	Kronecker's delta ($(\text{m}^{-1}), (\text{s}^{-1}), (\text{m}^{-1})$, respectively).
δt	time increment (s).
Δx	space increment (m).
γ	particle activity (random variable) (m).
κ	difference $\kappa = \sigma - \mu$ (s^{-1}).
λ	entrainment rate (s^{-1}).
$\tilde{\lambda}$	entrainment rate per unit length ($\text{m}^{-1} \text{s}^{-1}$).
λ'	volumetric entrainment rate (ms^{-1}).
μ	collective entrainment rate (s^{-1}).
ν	emigration rate (s^{-1}).
ρ	autocorrelation function.
ρ_p	particle density (kg m^{-3}).
σ	deposition rate (s^{-1}).

- ω_p particle volume (m^3).
- ξ Gaussian noise increment ($\text{s}^{-1/2}$).
- ξ_b space and time Gaussian noise increment ($\text{m}^{-1/2} \text{s}^{-1/2}$).

Acknowledgments

The work presented here was supported by the Swiss National Science Foundation under grants 200021-160083 (a project called “The Stochastic Torrent: Stochastic model for bed load transport on steep slope”) and 200021-105193/1 (a project called “Transient free-surface flows of concentrated suspensions—Application to geophysical flows,” funded by an R’Equip grant). Bohorquez acknowledges the financial support by the Caja Rural Provincial de Jaén and the University of Jaén (project UJA2014/07/04), École Polytechnique Fédérale de Lausanne (section de génie civil) and Junta de Andalucía (research stays from 2012 to 2014). We are grateful to Vaughan Voller, Editor John Buffington, and the Associate Editor for the numerous astute comments and helpful criticisms. Additional constructive remarks from anonymous reviewers have helped improve the presentation of the paper. The numerical data used in this paper were obtained using standard numerical techniques [Higham, 2001; Iacus, 2008], summarized in section 5 of the supporting information. This electronic supplement also includes the details of the mathematical developments and additional numerical simulations. All of the numerical simulations shown here were performed using Mathematica scripts (which are available upon request to Christophe Ancey, christophe.ancey@epfl.ch). Fortran 90 codes were also used to test the numerical methods (the corresponding codes can be obtained from Patricio Bohórquez, prmedina@ujaen.es). The data shown in Figure 1 are available from the *figshare* data repository: <http://dx.doi.org/10.6084/m9.figshare.1480646> (see also Appendix A).

References

- Allen, E. J. (2007), *Modeling with Itô Stochastic Differential Equations*, Springer, New York.
- Ancey, C. (2010), Stochastic modeling in sediment dynamics: Exner equation for planar bed incipient bed load transport conditions, *J. Geophys. Res.*, *115*, F00A11, doi:10.1029/2009JF001260.
- Ancey, C., and J. Heyman (2014), A microstructural approach to bed load transport: Mean behaviour and fluctuations of particle transport rates, *J. Fluid Mech.*, *744*, 129–168.
- Ancey, C., T. Böhm, M. Jodeau, and P. Frey (2006), Statistical description of sediment transport experiments, *Phys. Rev. E*, *74*, 011302.
- Ancey, C., A. C. Davison, T. Böhm, M. Jodeau, and P. Frey (2008), Entrainment and motion of coarse particles in a shallow water stream down a steep slope, *J. Fluid Mech.*, *595*, 83–114.
- Audusse, E., S. Boyaval, N. Goutal, M. Jodeau, and P. Ung (2015), Numerical simulation of the dynamics of sedimentary river beds with a stochastic Exner equation, *ESAIM: Proc. Surv.*, *48*, 321–340.
- Ballio, F., V. Nikora, and S. E. Coleman (2014), On the definition of solid discharge in hydro-environment research and applications, *J. Hydraul. Res.*, *52*, 173–184.
- Balmforth, N. J., and A. Provenzale (2001), Patterns of dirt, in *Geomorphological Fluid Mechanics*, edited by N. J. Balmforth and A. Provenzale, pp. 369–393, Springer, Berlin.
- Batchelor, G. K. (1974), Transport properties of two-phase materials with random structure, *Annu. Rev. Fluid Mech.*, *6*, 227–255.
- Bencala, K. E., and R. A. Walters (1983), Simulation of solute transport in a mountain pool-and-riffle stream: A transient storage model, *Water Resour. Res.*, *19*, 718–724.
- Blondeaux, P., G. Vittori, A. Bruschi, F. Lalli, and V. Pesarino (2012), Steady streaming and sediment transport at the bottom of sea waves, *J. Fluid Mech.*, *697*, 115–149.
- Boano, F., A. I. Packman, A. Cortis, R. Revelli, and L. Ridolfi (2007), A continuous time random walk approach to the stream transport of solutes, *Water Resour. Res.*, *43*, W10425, doi:10.1029/2007WR006062.
- Bohorquez, P., and C. Ancey (2015), Stochastic-deterministic modeling of bed load transport in shallow waterflow over erodible slope: Linear stability analysis and numerical simulation, *Adv. Water Res.*, *83*, 36–54.
- Buffington, J. (1999), The legend of A. Shields, *J. Hydraul. Eng.*, *125*, 376–387.
- Bunte, K., and S. Abt (2005), Effect of sampling time on measured gravel bed load transport rates in a coarse-bedded stream, *Water Resour. Res.*, *41*, W11405, doi:10.1029/2004WR003880.
- Campagnoli, J., A. Radice, and F. Ballio (2012), Scale-based statistical analysis of sediment fluxes, *Acta Geophys.*, *60*, 1744–1777.
- Charru, F. (2006), Selection of the ripple length on a granular bed sheared by a liquid flow, *Phys. Fluids*, *18*, 121508.
- Cox, D. R., and H. D. Miller (1965), *The Theory of Stochastic Processes*, Chapman and Hall CRC, Boca Raton, Fla.
- Crank, J. (1975), *The Mathematics of Diffusion*, Oxford Univ. Press, Oxford.
- Cudden, J. R., and T. B. Hoey (2003), The causes of bedload pulses in a gravel channel: The implications of bedload grain-size distributions, *Earth Surf. Processes Landforms*, *28*, 1411–1428.
- Culling, W. E. H. (1960), Analytical theory of erosion, *J. Glaciol.*, *68*, 336–344.
- Dogan, E., and E. J. Allen (2011), Derivation of stochastic partial differential equations for reaction-diffusion processes, *Stoch. Anal. Appl.*, *29*, 424–443.
- Einstein, H. A. (1950), The bed-load function for sediment transportation in open channel flows, *Tech. Rep. 1026*, U.S. Dept. of Agriculture, Washington, D. C.
- Fan, N., D. Zhong, B. Wu, E. Fofoula-Georgiou, and M. Guala (2014), A mechanistic-stochastic formulation of bed load particle motions: From individual particle forces to the Fokker-Planck equation under low transport rates, *J. Geophys. Res. Earth Surf.*, *119*, 464–482, doi:10.1002/2013JF002823.
- Ferguson, R. I., and M. Church (2009), A critical perspective on 1-D modeling of river processes: Gravel load and aggradation in lower Fraser River, *Water Resour. Res.*, *45*, W11424, doi:10.1029/2009WR007740.
- Fofoula-Georgiou, E., V. Ganti, and W. E. Dietrich (2010), A nonlocal theory of sediment transport on hillslopes, *J. Geophys. Res.*, *115*, F00A16, doi:10.1029/2009JF001280.
- Furbish, D. J., and P. K. Haff (2010), From divots to swales: Hillslope sediment transport across diverse length scales, *J. Geophys. Res.*, *115*, F03001, doi:10.1029/2009JF001576.
- Furbish, D. J., and J. J. Roering (2013), Sediment disentrainment and the concept of local versus nonlocal transport on hillslopes, *J. Geophys. Res. Earth Surf.*, *118*, 937–952, doi:10.1002/jgrf.20071.
- Furbish, D. J., and M. W. Schmeeckle (2013), A probabilistic derivation of the exponential-like distribution of bed load particle velocities, *Water Resour. Res.*, *49*, 1537–1551, doi:10.1002/wrcr.20074.
- Furbish, D. J., J. C. Roseberry, and M. W. Schmeeckle (2012a), A probabilistic description of the bed load sediment flux: 3. The particle velocity distribution and the diffusive flux, *J. Geophys. Res.*, *117*, F03033, doi:10.1029/2012JF002355.
- Furbish, D. J., P. K. Haff, J. C. Roseberry, and M. W. Schmeeckle (2012b), A probabilistic description of the bed load sediment flux: 1. Theory, *J. Geophys. Res.*, *117*, F03031, doi:10.1029/2012JF002352.
- Furbish, D. J., A. E. Ball, and M. W. Schmeeckle (2012c), A probabilistic description of the bed load sediment flux: 4. Fickian diffusion at low transport rates, *J. Geophys. Res.*, *117*, F03034, doi:10.1029/2012JF002356.
- Gabet, E. J., and M. K. Mendoza (2012), Particle transport over rough hillslope surfaces by dry ravel: Experiments and simulations with implications for nonlocal sediment flux, *J. Geophys. Res.*, *117*, F01019, doi:10.1029/2011JF002229.
- Gaeuman, D., C. R. Holt, and K. Bunte (2015), Maximum likelihood parameter estimation for fitting bedload rating curves, *Water Resour. Res.*, *51*, 281–301, doi:10.1002/2014WR015872.
- Ganti, V., M. M. Meerschaert, E. Fofoula-Georgiou, E. Viparelli, and G. Parker (2010), Normal and anomalous diffusion of gravel tracer particles in rivers, *J. Geophys. Res.*, *115*, F00A12, doi:10.1029/2008JF001222.
- García, M. H. (2007), Sediment transport and morphodynamics, in *Sedimentation Engineering*, edited by M. H. García, pp. 21–164, ASCE Manuals and Reports on Engineering Practice 110, Am. Soc. of Civil Engineers, Reston, Va.
- Gardiner, C. W. (1983), *Handbook of Stochastic Methods*, Springer, Berlin.

- Gillespie, D. T. (1992), *Markov Processes: An Introduction for Physical Scientists*, Academic Press, San Diego, Calif.
- Gillespie, D. T. (2001), Approximate accelerated stochastic simulation of chemically reacting systems, *J. Chem. Phys.*, *115*, 1716–1733.
- Gillespie, D. T., and E. Seitaridou (2013), *Simple Brownian Diffusion*, Oxford Univ. Press, Oxford.
- Gomez, B. (1991), Bedload transport, *Earth Sci. Rev.*, *31*, 89–132.
- Guazzelli, E., and J. F. Morris (2012), *A Physical Introduction to Suspension Dynamics*, Cambridge Univ. Press, Cambridge.
- Hairer, M., and J. Voss (2011), Approximations to the stochastic Burgers equation, *J. Nonlinear Sci.*, *21*, 897–920.
- Heimsath, A. M., D. J. Furbish, and W. E. Dietrich (2005), The illusion of diffusion: Field evidence for depth-dependent sediment transport, *Geology*, *33*, 949–952.
- Hellander, S., A. Hellander, and L. Petzold (2012), Reaction-diffusion master equation in the microscopic limit, *Phys. Rev. E*, *85*, 042901.
- Heyman, J. (2014), A study of the spatio-temporal behaviour of bed load transport rate fluctuations, PhD thesis, École Polytechnique Fédérale de Lausanne, Lausanne, Switzerland.
- Heyman, J., F. Mettra, H. B. Ma, and C. Ancey (2013), Statistics of bedload transport over steep slopes: Separation of time scales and collective motion, *Geophys. Res. Lett.*, *40*, 128–133, doi:10.1029/2012GL054280.
- Heyman, J., H. B. Ma, F. Mettra, and C. Ancey (2014), Spatial correlations in bed load transport: Evidence, importance, and modeling, *J. Geophys. Res. Earth Surf.*, *119*, 1751–1767, doi:10.1002/2013JF003003.
- Higham, D. J. (2001), An algorithmic introduction to numerical simulation of stochastic differential equations, *SIAM Rev.*, *43*, 525–546.
- Hill, K. M., L. Dell'Angelo, and M. M. Meerschaert (2010), Heavy-tailed travel distance in gravel bed transport: An exploratory enquiry, *J. Geophys. Res.*, *115*, F00A14, doi:10.1029/2009JF001276.
- Hodge, R. A., and T. B. Hoey (2012), Upscaling from grain-scale processes to alluviation in bedrock channels using a cellular automaton model, *J. Geophys. Res.*, *117*, F01017, doi:10.1029/2011JF002145.
- Iacus, S. M. (2008), *Simulation and Inference for Stochastic Differential Equations*, Springer, New York.
- Isaacson, S. A. (2005), The reaction-diffusion master equation as an asymptotic approximation of diffusion to a small target, *SIAM J. Appl. Math.*, *70*, 77–111.
- Lajeunesse, E., L. Malverti, and F. Charru (2010), Bed load transport in turbulent flow at the grain scale: Experiments and modeling, *J. Geophys. Res.*, *115*, F04001, doi:10.1029/2009JF001628.
- Lajeunesse, E., O. Devauchelle, M. Houssais, and G. Seizilles (2013), Tracer dispersion in bedload transport, *Adv. Geosci.*, *37*, 1–6.
- LeVeque, R. J. (2002), *Finite Volume Methods for Hyperbolic Problems*, Cambridge Univ. Press, Cambridge.
- Lipshtat, A. (2007), "All possible steps" approach to the accelerated use of Gillespie's algorithm, *J. Chem. Phys.*, *126*, 184103.
- Majda, A. J., and P. R. Kramer (1999), Simplified models for turbulent diffusion: Theory, numerical modelling, and physical phenomena, *Phys. Rep.*, *314*, 237–574.
- Martin, R. L., D. J. Jerolmack, and R. Schumer (2012), The physical basis for anomalous diffusion in bed load transport, *J. Geophys. Res.*, *117*, F01018, doi:10.1029/2011JF002075.
- Martin, Y. (2000), Modelling hillslope evolution: Linear and nonlinear transport relations, *Geomorphology*, *34*, 1–21.
- Méndez, V., S. Fedotov, and W. Horsthemke (2010), *Reaction-Transport Systems: Mesoscopic Foundations, Fronts, and Spatial Instabilities*, Springer, Berlin.
- Mettra, F. (2014), Morphodynamic mechanisms in steep channels: From local processes to large-scale evolution, PhD thesis, École Polytechnique Fédérale de Lausanne, Lausanne, Switzerland.
- Metzler, R., and J. Klafter (2000), The random walk's guide to anomalous diffusion: A fractional dynamics approach, *Phys. Rep.*, *339*, 1–77.
- Narteau, C., D. Zhang, O. Rozier, and P. Claudin (2009), Setting the length and time scales of a cellular automaton dune model from the analysis of superimposed bed forms, *J. Geophys. Res.*, *114*, F03006, doi:10.1029/2008JF001127.
- Nikora, V., H. Habersack, T. Huber, and I. McEwan (2002), On bed particle diffusion in gravel bed flows under weak bed load transport, *Water Resour. Res.*, *38*(6), 17–1–17-9, doi:10.1029/2001WR000513.
- Oh, J., and C. W. Tsai (2010), A stochastic jump diffusion particle-tracking model (SJD-PTM) for sediment transport in open channel flows, *Water Resour. Res.*, *46*, W10508, doi:10.1029/2009WR008443.
- Paola, C. (2000), Quantitative models of sedimentary basin filling, *Sedimentology*, *47*, 121–178.
- Paola, C. (2011), Simplicity versus complexity, *Nature*, *469*(7328), 38–39.
- Parker, G., C. Paola, and S. Leclair (2000), Probabilistic Exner sediment continuity equation for mixtures with no active layer, *J. Hydraul. Eng.*, *126*, 818–826.
- Pelosi, A., G. Parker, R. Schumer, and H. B. Ma (2014), Exner-based Master Equation for transport and dispersion of river pebble tracers: Derivation, asymptotic forms, and quantification of nonlocal vertical dispersion, *J. Geophys. Res. Earth Surf.*, *119*, 1818–1832, doi:10.1002/2014JF003130.
- Pineda-Krch, M. (2008), GillespieSSA: implementing the stochastic simulation algorithm in R, *J. Stat. Softw.*, *25*, 1–18.
- Platen, E. (1999), An introduction to numerical methods for stochastic differential equations, *Acta Numer.*, *8*, 197–246.
- Pope, S. B. (2000), *Turbulent Flows*, Cambridge Univ. Press, Cambridge.
- Pusey, P. N. (2011), Brownian motion goes ballistic, *Science*, *332*, 802–803.
- Recking, A., F. Liébault, C. Peteuil, and T. Jolimet (2012), Testing bedload transport equations with consideration of time scales, *Earth Surf. Processes Landforms*, *37*, 774–789.
- Reitz, M. D., D. J. Jerolmack, E. Lajeunesse, A. Limare, O. Devauchelle, and F. Métévier (2014), Diffusive evolution of experimental braided rivers, *Phys. Rev. E*, *89*, 052809.
- Ridolfi, L., P. D'Odorico, and F. Laio (2011), *Noise-Induced Phenomena in the Environmental Sciences*, Cambridge Univ. Press, Cambridge.
- Roseberry, J. C., M. W. Schmeeckle, and D. J. Furbish (2012), A probabilistic description of the bed load sediment flux: 2. Particle activity and motions, *J. Geophys. Res.*, *117*, F03032, doi:10.1029/2012JF002353.
- Salles, T., and G. Duclaux (2015), Combined hillslope diffusion and sediment transport simulation applied to landscape dynamics modelling, *Earth Surf. Processes Landforms*, *40*, 823–839.
- Schumer, R., M. M. Meerschaert, and B. Bauemer (2009), Fractional advection-dispersion equations for modeling transport at the Earth surface, *J. Geophys. Res.*, *114*, F00A07, doi:10.1029/2008JF001246.
- Seizilles, G., E. Lajeunesse, O. Devauchelle, and M. Bak (2014), Cross-stream diffusion in bedload transport, *Phys. Fluids*, *26*, 013302.
- Seminara, G. (2010), Fluvial sedimentary patterns, *Annu. Rev. Fluid Mech.*, *42*, 43–66.
- Singh, A., K. Fienberg, D. J. Jerolmack, J. Marr, and E. Fofoula-Georgiou (2009), Experimental evidence for statistical scaling and intermittency in sediment transport rates, *J. Geophys. Res.*, *114*, F01025, doi:10.1029/2007JF000963.
- Sun, H. G., D. Chen, Y. Zhang, and L. Chen (2015), Understanding partial bed-load transport: Experiments and stochastic model analysis, *J. Hydrol.*, *521*, 196–204.
- Toro, E. F. (2001), *Shock-Capturing Methods for Free-Surface Shallow Flows*, Wiley, Chichester.

- Tsai, C. W., Y. Hsu, K. C. Lai, and N. K. Wu (2014), Application of gambler's ruin model to sediment transport problems, *J. Hydrol.*, *510*, 197–207.
- Tucker, G. E., and D. N. Bradley (2010), Trouble with diffusion: Reassessing hillslope erosion laws with a particle-based model, *J. Geophys. Res.*, *115*, F00A10, doi:10.1029/2009JF001264.
- van Rijn, L. C. (2007), Unified view of sediment transport by currents and waves. II: Suspended transport, *J. Hydraul. Eng.*, *133*, 668–689.
- Wu, W. (2007), *Computational River Dynamics*, Taylor and Francis, London.
- Zhang, Y., M. M. Meerschaert, and A. I. Packman (2012), Linking fluvial bed sediment transport across scales, *Geophys. Res. Lett.*, *39*, L20404, doi:10.1029/2012GL053476.